Spectrally Resolved Synthetic Aperture Imaging Interferometer

Final Report of NASA Innovative Advanced Concepts
Phase 1 Study
17-NIAC18B-0145

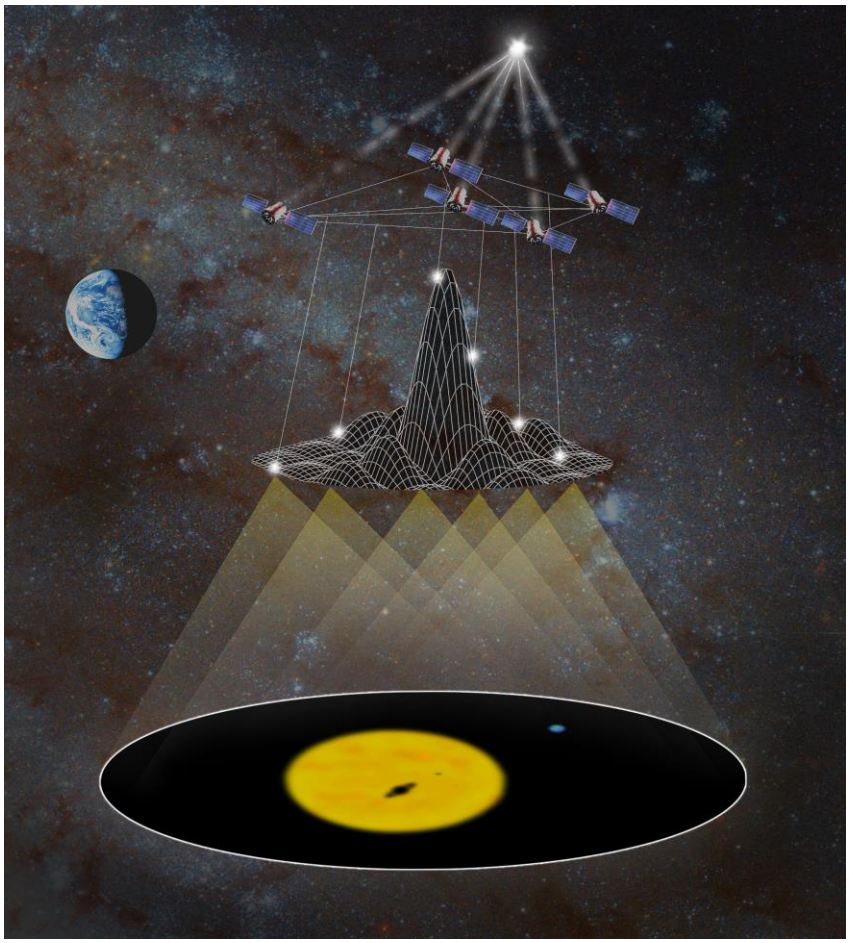

Jordan Wachs[1] (PI)
Jennifer Lee[1], Roger Linfield[1], Jeff Kommers[1], Webster Cash[2]

January 25, 2019

[1]Ball Aerospace, Boulder, CO, 80301
[2]Center for Astrophysics and Space Astronomy, University of Colorado Boulder, Boulder, CO, 80309

Table of Contents

Figures

Acronym List

Acronym	Meaning
BETTII	The Balloon Experimental Twin Telescope for Infrared Interferometry
BW	Bandwidth
DARPA	Defense Advanced Research Projects Agency [now ARPA]
DFACS	Drag-Free and Attitude Control System
GB	Gigabyte
HST	Hubble Space Telescope
JWST	James Webb Space Telescope [formerly NGST]
LISA	Laser Interferometer Space Antenna
LO	Local Oscillator
LUVOIR	Large UV Optical and InfraRed
MOIRE	Membrane Optic Imager Real-Time Exploitation
NASA	National Aeronautics and Astronautics Administration
NIAC	NASA Innovative Advanced Concepts
NIST	National Institute of Standards and Technology [formerly NBS]
PI	Principal Investigator
PIC	Photonic Integrated Circuit
RF	Radio Frequency
RMS	Root-Mean-Square
SNR	Signal-to-Noise Ratio
SNSPD	Superconducting Nanowire Single Photon Detector
SRSAII	Spectrally Resolved Synthetic Aperture Imaging Interferometer
SWAP	Size, Weight, and Power
UV	Ultraviolet
VLBI	Very-long-Baseline Interferometry

1. Executive Summary

The Spectrally Resolved Synthetic-Aperture Imaging Interferometer (SRSAII) is a system proposed to provide high-resolution and high-sensitivity measurements of astronomical objects. SRSAII uses long baseline interferometric methods to achieve the resolution and low-noise, high time-precision detection to achieve the sensitivity.

The primary goal of the SRSAII study was to lay out a framework for using new optical physics technologies to directly resolve, both spatially and spectrally, the disk of an exoplanet. In addition to the ambitious goal of directly resolving an exoplanet, the SRSAII team also sought to identify science opportunities achievable with intermediate system configurations which may offer resolution significantly higher than the current state of the art, but insufficient for direct resolution of an exoplanetary disk.

An operational SRSAII system can function with essentially arbitrarily large baselines, achieving correspondingly high angular resolution. The primary limitation occurs in the system sensitivity, which became the major technical focus for study. In this report, we compare the predicted performance (sensitivity in SNR along with angular resolution) of three interferometric techniques: direct detection (also known as homodyne interferometry), multi-channel intensity interferometry (using the Hanbury Brown and Twiss effect), and multi-channel heterodyne interferometry (using an optical frequency comb as a local oscillator). Additionally, quantum-assisted interferometry is also explored as a prospective enhancement of established methods.

This report presents a survey of the technologies that enable the SRSAII techniques -- optical frequency combs, single photon detectors, and photonic integrated circuits. These technologies are the basis of methods critical to SRSAII's success: precision timing, length and frequency metrology, sensitive photodetection, fine-scale wavelength filtering, and dense multi-channel operation. Lastly, we give some notional performance metrics and propose some possible experimental observations.

1.1. Background and Motivation

The basic function optical telescopes have remained essentially unchanged since its purported "first use" by Galileo for observing astronomical objects – larger optics for better light collection and resolution, wave-front control for more precise focusing, better detectors for more sensitive measurement. Multi-aperture techniques common for radio frequency (RF) observations such as direct-detection (homodyne) interferometry or Very-long-baseline interferometry (VLBI) have seen limited use in the optical domain due to several technological hurdles: optical path control, phase reference stability, and detector bandwidths. Recent advances in optical and detector physics have opened the door to measurement and control of the electromagnetic field at optical frequencies with such precision that techniques developed for the radio domain can be applied to the optical. Leveraging these techniques to create an optical very long baseline interferometer offers a viable path toward ultra-high-resolution images of distant astronomical targets.

The Ball team has identified a method in which discriminating technologies, Optical Frequency Combs, Photonic Integrated Circuits (PICs), and ultra-high time precision single photon detectors, allow creation of a digital long-baseline optical interferometer which can achieve the

same angular resolution as a direct-detection (homodyne) interferometer, but is not limited by the optical control requirements of the traditional technique. Where the complexity of a direct-detection interferometer increases as baselines grow larger, SRSAII is not fundamentally limited in the baseline length because detection happens before aperture combination (correlation). By reducing the interferometry to a digital post-processing problem requiring precise distance and timing knowledge, but not control, one can bypass the difficulties of interferometric beam combination.

The Spectrally Resolved Synthetic Aperture Imaging Interferometer (SRSAII) is a synthetic aperture imaging interferometer, which reconstructs an image by sampling the Fourier space (u, v plane) with a multitude of individual apertures. The signal at each aperture can be collected as either an intensity distribution in time, or first mixed with a frequency reference (local oscillator, LO) and then the beat signal detected. In this report we will refer to these strategies as intensity interferometry and heterodyne interferometry, respectively. Signals from individual apertures can then be correlated in post-processing to extract coincidence features, which reveal the field distribution in space.

Dividing the collected spectrum into many narrow channels using a PIC makes the correlation easier and the parallel measurement of many channels improves the signal to noise ratio. The spectral references are taken from the optical frequency comb, which provides exquisite frequency stability and broadband phase coherence of each of the comb's 'teeth', or frequency components. Combs make possible coherent detection and digitization over a full octave or more of optical spectrum, dramatically increasing the signal to noise ratio (SNR) for a heterodyne interferometer (using frequency comb generated LOs).[1] The process of heterodyne interferometry down-converts optical-frequency oscillations at hundreds of terahertz (10^{14} Hz) into manageable signals in the gigahertz (10^{9} Hz) domain, where mature detection and processing technologies exist. Using the repeating spectrum of the frequency comb, it is possible to divide large portions of the electromagnetic spectrum into narrow channels, each with its own local oscillator.

Decomposing the optical field in this manner traditionally requires an ability to deal with enormous data volumes. Nyquist sampling of the field between 500 nm and 2 μm requires a minimum data rate of hundreds of Tb/sec. Despite the rapid advancements in data collection and processing, this is still an unwieldly number well beyond reasonable expectations for the near future. In the low photon flux regime, however, the use of photon counting detectors with high temporal precision allows us to invert the measurement, only recording data when a photon is detected. The detector temporal resolution, t_r, allows an effective detector bandwidth of $1/t_r$, but only requires a data rate proportional to the photon flux, which is much lower than the Nyquist sampling rate. Using this detection scheme, SRSAII anticipates data rates on the order of 10s of Gb/sec, which is an improvement of 10^4 compared to Nyquist sampling of the full optical field with a traditional detector.

1.2. Findings

The SRSAII phase 1 NIAC study envisioned a long-baseline interferometry mission to directly resolve exoplanets. Detailed investigation of the signal-to-noise picture of an interferometer that leverages optical frequency combs and advanced photon counting detectors in a severely photon-starved regime yielded promising results. As this study did not include rigorous system design studies, SNR values for each detection process assume ideal detection efficiency. This allows direct comparison of each technique, shown in **Figure 1**, without imposing assumptions about any individual technology.

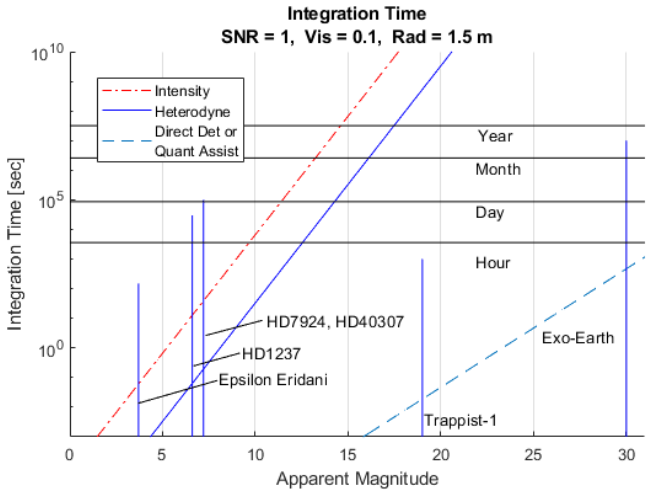

Figure 1: Integration times required to resolve diameter of astronomical target as a function of apparent magnitude. Included are all four interferometry methods investigated in the SRSAII phase 1 NIAC study: Intensity, Heterodyne, Direct Detect, and Quantum Assisted Interferometry.

Implementation of a multi-channel frequency comb-based detection scheme allowed a significant increase in optical bandwidth for the SRSAII system, which substantially decreases the required observation time to achieve SNR goals when compared to other approaches. Both intensity and heterodyne interferometry techniques saw an improvement factor of approximately 10^4 in required integration time when compared to present-day efforts.[2,3]

Independent calculation of the SNR using classical electrodynamics[4] and a semi-classical approach[5] revealed that substantial improvement can be realized with the SRSAII architecture. While our findings suggest observation in the low-photon regime is impractical with intensity interferometry, the SRSAII optical heterodyne interferometry architecture can resolve targets as deep as the 15th magnitude using 3m collecting optics, arbitrarily large baselines, reasonable data rates, and acceptable integration times.

Despite significant improvement over the state of the art, the SRSAII architecture is still limited due to the classical Fourier analysis it performs. The quantum mechanical perspective, which takes into account quantum information theory and quantum-mechanical detection and correlation techniques, confirms the limits on the classical system, but also offer insight into methods which bypass the classical constraints using quantum Fourier techniques. These techniques, while technically challenging, offer a potentially viable path toward improvement of the SRSAII system SNR to make possible resolution of targets as dim as 30th magnitude.

2. History and Motivation

2.1. Desire for Increased Angular Resolution

Angular resolution, which is one of the most critical aspects of any astronomical observation is given by the well-known Rayleigh criterion formula:

$$\theta_r = 1.22\frac{\lambda}{d} \quad (1)$$

which states that the minimum resolvable angle between two objects is proportional to the wavelength, λ , over the diameter of the telescope, d. This linear relationship between telescope diameter and angular resolution has consistently driven the science community toward larger optical diameters.

Increasing the diameter of a telescope allows it to observe finer detail but comes with added cost and complexity, especially for space-based telescopes. The 2.5m diameter Hubble Space Telescope (HST) is capable of observing features as small as 40 milliarcseconds (mas) and the upcoming James Webb Space Telescope (JWST) will achieve up to 18 mas resolution with its 6.5m diameter optic. DARPA funded the MOIRE program, which intended to create 20m diffraction limited optics[6]. See **Figure 2** for size comparisons.

Despite these advances, astronomical targets still commonly exhibit structures on much smaller angular scales than can be observed with HST or JWST. To obtain multiple resolution elements across a spectral type B star, for instance, would require a telescope with a diameter on the order of approximately 1km. At more than 150 times the diameter of JWST, a continuous aperture telescope of this size is exceptionally difficult with modern or foreseeable technologies.

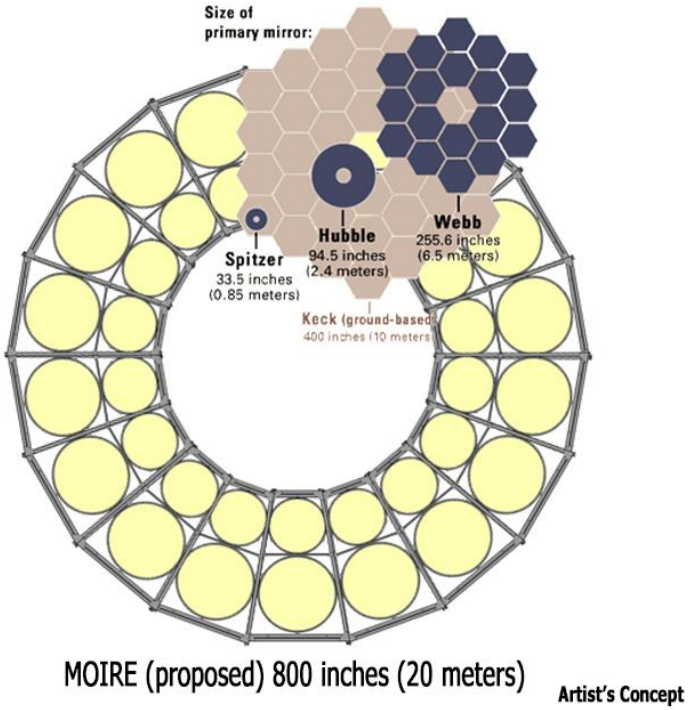

Figure 2: Illustration of the physical sizes of existing (Spitzer and Hubble), planned (Webb) and potential future (MOIRE) space-based telescopes.[6]

An alternative to a continuous aperture telescope is interferometry, which offers great promise for the creation of observatories capable of directly resolving such structures. This technique allows the linking of multiple small telescopes to form a virtual aperture with a maximum angular resolution that is determined by the maximum dimension of the telescope arrangement, rather than the diameter of any of its component telescopes. A constellation with a maximum dimension of 1km could therefore be

used to construct multiple resolution elements across an object such as a spectral type B star without the need for extremely large optical assemblies.

2.2. The diffraction limit and larger telescopes.

An optical telescope is said to be performing at the 'diffraction limit' when it collects and focuses light so precisely that its imaging performance is limited by the natural behavior of the optical field rather than any imperfections in the optical system. For a system to attain diffraction limited performance, it is necessary for its optical surfaces to be shaped and positioned to precisions significantly less than the wavelength of the sampled light. For a telescope operating at optical wavelengths, this requires surface quality and mechanical tolerances of a few tens of nanometers. While manufacturing techniques and processes routinely accomplish this for smaller optics, costs quickly grow to unmanageable levels when telescope diameters exceed a few meters in diameter.

The cost growth associated with increased diameter is a major challenge for creating large telescopes, especially in space. To ensure diffraction-limited performance of its 6-meter aperture, the James Webb Space Telescope (JWST) primary telescope assembly uses more than 120 actuators to make fine adjustments on each of the 18 mirror segments, each of which has been polished to RMS roughness of less than 20nm. The Large UV Optical and InfraRed (LUVOIR) explorer, one of the next generation multi-segmented telescope concepts currently undergoing preliminary trades by NASA Science and Technology Definition Teams, is greatly stressing modern technology to offer a diffraction-limited aperture of twice the diameter of JWST.[7]

2.3. What is a telescope really doing?

In order to understand alternatives to the traditional telescope, it is helpful first to understand the basic function of the optical telescope. From a fundamental perspective, a telescope collects light from different points across its primary optic and focuses the light onto a detector. The focusing process itself, while relatively simple to model, is somewhat complicated to picture. The focusing mechanism combines the optical field in such a way that when it lands on the detector, it performs a correlation between the phase information collected by each section of the aperture and that collected by every other segment of the aperture. This results in the continuous cross-correlation of the field across the full optical surface, resulting in a fully sampled image of the source.[8]

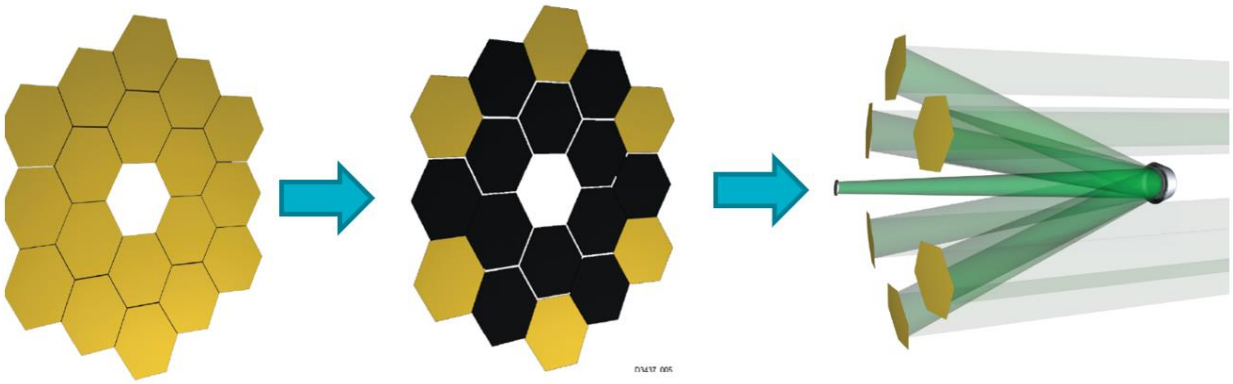

Figure 3: A traditional telescope mirror (left) is a filled aperture, whereas an interferometer (right) only partially samples the aperture.

While this picture of the operation of a telescope is nontraditional, it provides a convenient perspective from which to investigate interferometry: It is the information collected on the *phase correlation* across the telescope aperture that forms an image. Use of a traditional, continuous, aperture maximizes the gathered signal and greatly decreases the complexity of the image formation process.

Due to the simplicity of construction and operation, a continuous aperture is the preferred approach for smaller systems. For large systems, however, a *sparse* aperture can be created by coordinate smaller sub-apertures to effectively form a single large aperture as shown in **Figure 3**. By replacing a single large optical surface with multiple smaller ones, it is possible to space out the optics in such a way as to increase the effective resolution of the system while greatly decreasing system mass. Additional complexities arise when implementing sparse apertures, however they have recently become feasible in a wide range of contexts.

2.4. Optical Interferometry

Optical interferometry is a technique which achieves essentially the same measurement as a traditional telescope, but without the requirement of a continuous optical surface to collect light. Interferometry can be thought of as a natural extension from traditional imaging in that a telescope with a surface that is partially obscured, as shown in **Figure 4**, is functionally collecting light from multiple discrete areas and interfering it on a focal plane. Continuing with this concept, it is possible to separate the collecting optics by increasingly large distances, called baselines, shown at bottom right in Figure 4.[9]

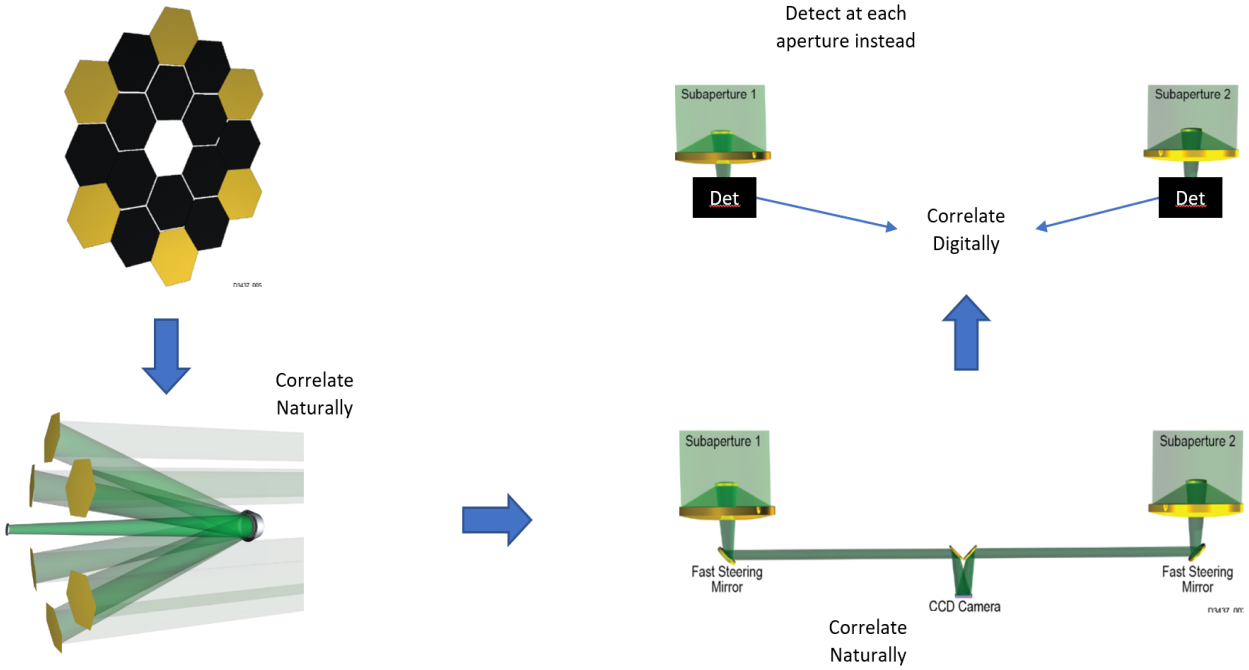

Figure 4: Evolution of a sparse aperture from a partially obstructed mirror (top left) to a sparse aperture direct detection interferometer (bottom left to bottom right) and finally to a heterodyne interferometer (top right).

When enough care is taken to design the optical path between the points of collection and detection, it is possible for the collecting optics, or sub-apertures, to be on separate structures or even free-flying spacecraft. This allows baselines on the order of tens to hundreds of meters. This technique, where optical fields from distant telescopes are coherently combined, is called direct detection interferometry, is very sensitive but suffers from added complexity due to elaborate optomechanical engineering associated with designing the optics which coherently combine each pair of optical beams. Furthermore, significant transmission losses can occur due to beam diffraction for long baselines.

While less sensitive than direct detection interferometry, other techniques such as intensity interferometry and heterodyne interferometry allow light to be detected at each sub-aperture rather than physically propagating precisely controlled light along a designed path from the collector to a common detector. This key distinction allows the information in the light collected at each sub-aperture to be correlated with that of the light collected at every other sub-aperture digitally. Detection at each sub-aperture and subsequent correlation of the digitized signals eliminates inter-spacecraft transmission losses suffered by direct detection interferometers. Digital correlation allows lossless combination of measured signal from an unlimited number of sub-apertures, enabling extremely long baselines and extraordinary angular resolution.

As can be seen in **Figure 5** the SRSAII system performs the latter types of interferometry, offering a digital version of every process performed by a traditional telescope or direct-detect interferometer. In both cases, the light is collected at multiple sub-apertures, the phase information correlated, and an image of the source is created through the Fourier relationships intrinsic to all optical imaging systems.

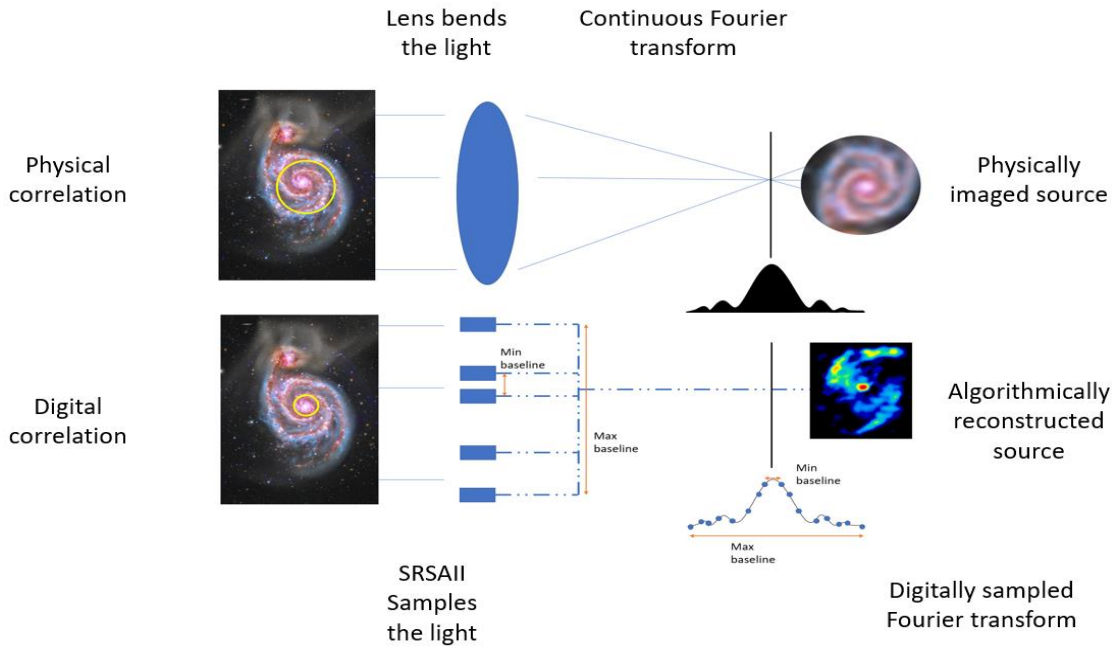

Figure 5: Illustration of the difference between direct imaging and heterodyne interferometric imaging. In direct imaging (top), a telescope generates an image with a lens or mirror. In heterodyne interferometric imaging, light from different parts of the aperture is sampled, mixed, recorded, and then digitally correlated in software. Color image[10], Interferometric reconstruction[11]

3. SRSAII

The SRSAII architecture is capable of performing both heterodyne and intensity interferometry, however real-world implementation will require system optimization for one or the other to fully take advantage of the benefits of each technique. The primary emphasis for SRSAII is on long baseline optical heterodyne interferometry, though it is also noted that the parallel channel detection implemented by SRSAII promises to significantly improve the sensitivity of intensity interferometers in the optical domain.

3.1. Science enabled by SRSAII

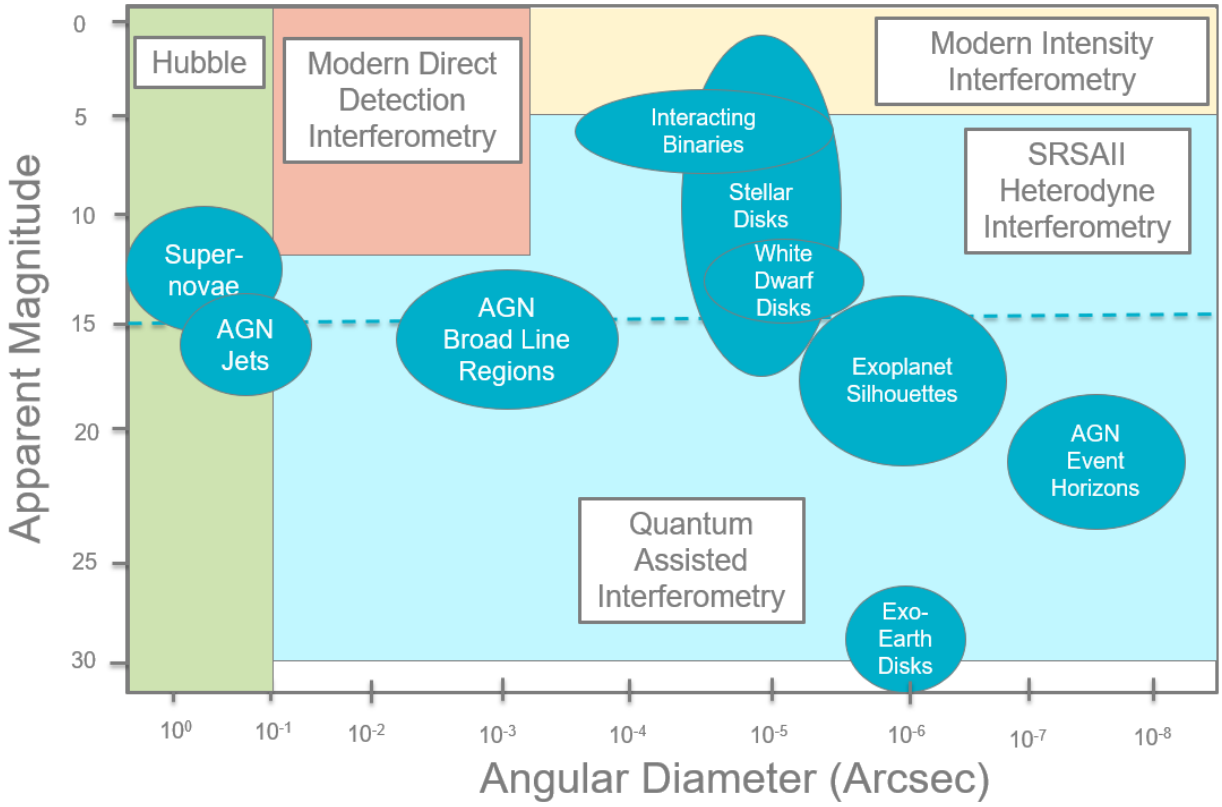

Figure 6: Bubble chart showing new observations possible with SRSAII.

Non-traditional interferometry has the potential to greatly improve on the angular resolution achievable with current observation techniques in the optical and NIR domains. **Figure 6** shows a comparison of techniques, showing sensitivity and achievable angular resolution. Modern Direct Detection figure is based on the Chara array, with a 300m maximum baseline and sensitivity to 12th magnitude.[12] Approaches studied by the SRSAII team are shown in blue, with the dashed line separating the SRSAII heterodyne approach from the potential performance of a quantum-assisted interferometer. The SRSAII heterodyne approach, which is achievable laboratory proven techniques, offers a path toward multi-kilometer baselines and high spectral resolution without the beam combination limitations of modern direct detection interferometers.

3.2. High Level System Architecture

SRSAII consists of a number, *n*, of free-flying spacecraft stabilized at an earth-sun Lagrange point (see **Figure 7**). Each spacecraft is capable of coherently detecting and digitally recording the optical field received from a distant astronomical source and possesses its own detection hardware which operates independently of all other spacecraft in the constellation. Metrology information that defines the location of each spacecraft with respect to the constellation is recorded in parallel with the optical field, and the optical field recovered at each spacecraft is correlated in post-processing.

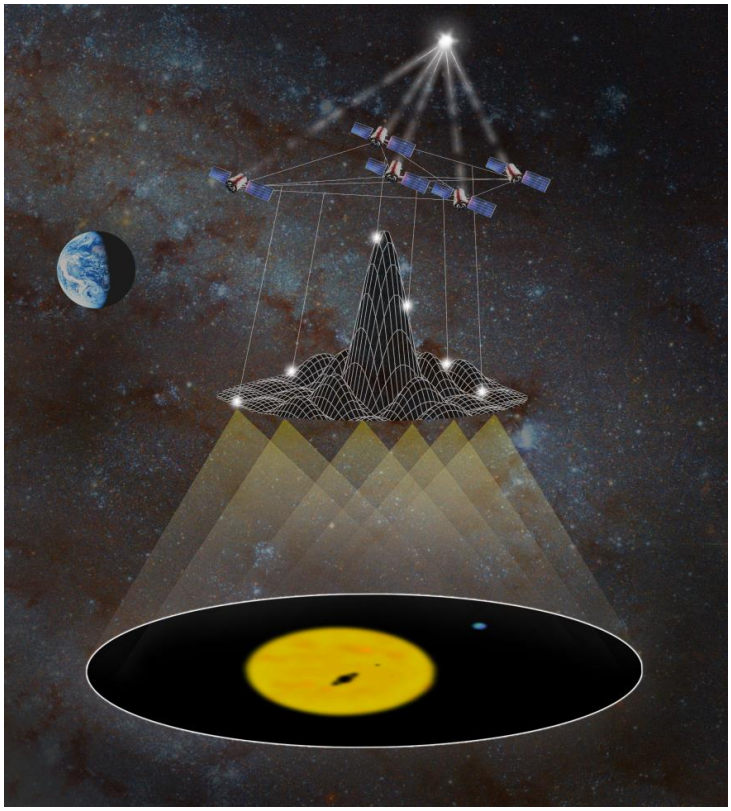

Figure 7: Artist's concept of a constellation of multiple spacecraft observing a source simultaneously, with data used from all telescopes to generate an image with greatly superior angular resolution than that possible with any individual telescope.

Digital correlation avoids the need for optical combination of the received signal and allows use of all $n(n-1)/2$ baselines without the reconfiguration of hardware upon addition or subtraction of spacecraft within the constellation. This gives mission operators the ability to reconfigure the constellation adding or removing spacecraft as required.

Primarily intended to image faint targets, SRSAII employs ultra-high temporal resolution photon counting detectors which offer single photon sensitivity and data rates proportional the photon detection rate rather than total detected optical bandwidth. This critical distinction reduces anticipated data rates by many orders of magnitude from hundreds Tb/sec to a much more manageable tens of GB/sec.

The optical frequency comb on each spacecraft gives a metrology reference as well as providing a bank of local oscillators (LOs) for heterodyne detection. Offering a continuous spectrum of equally spaced LOs, the frequency combs allow spectral resolution of $R > 10^5$ across the full wavelength region of 500nm to 2000nm. Optical channelization, field combination, and heterodyne detection are done with photonic integrated circuits, which offer significantly decreased size weight and power (SWAP) when compared to free space or fiber optic techniques.

3.3. High Level Detector Architecture Description

The SRSAII system consists of a constellation of many spacecraft, each of which is equipped with a telescope, frequency comb local oscillator (LO) bank, and array of high-precision single photon detectors (see **Figure 9**). Each spacecraft measures and records the optical field amplitude and phase by coherently combining the sampled light from each channel with its respective LO (comb tooth), providing enough information to allow for digital cross-correlation of the received signals in post-processing. Optical routing, mixing, and frequency comb generation is conducted on photonic integrated circuits (PICs), shown in **Figure 8**, which offer the ability to handle hundreds of distinct optical signals in a centimeter-scale package.

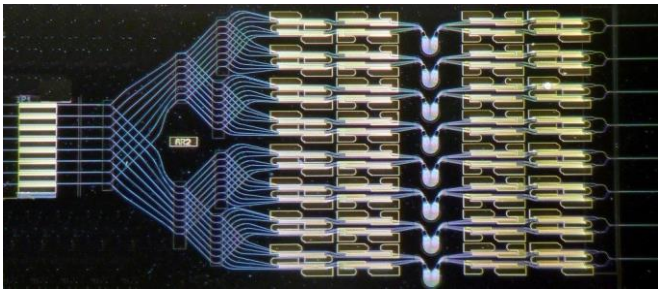

Figure 8: Photonic Integrated Circuit (PIC) encorporating 200 optical components on a single chip measuing 7mm x 15mm.[13] This PIC provides general signal routing and does not include a comb.

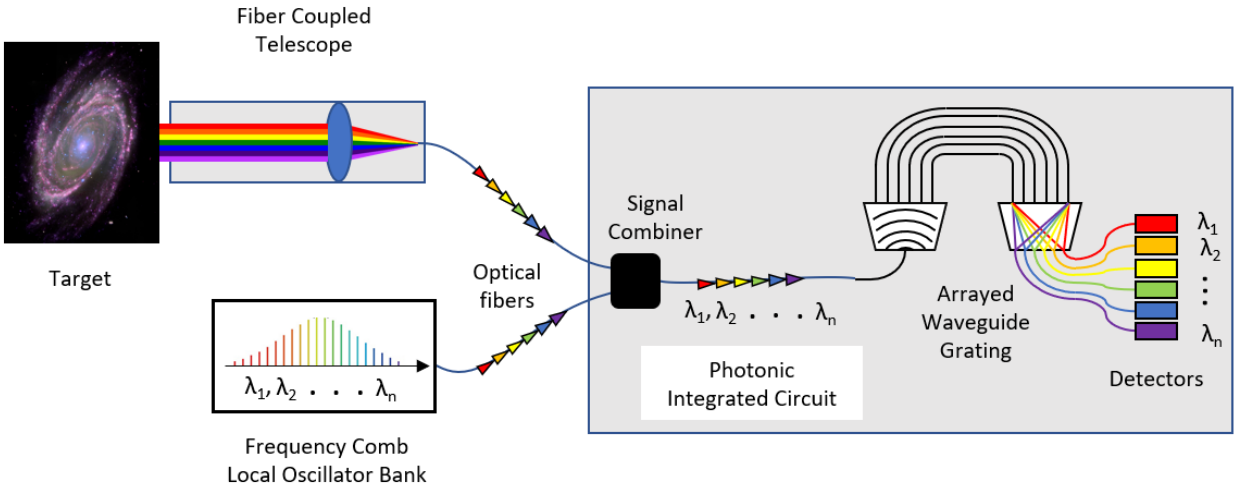

Figure 9: Schematic of the SRSAII concept. Light from a telescope is collected and mixed with light from a frequency comb. The combined light is then dispersed into many spectral channels by an arrayed waveguide grating and subsequently detected by a bank of detectors. The signal combination, dispersion, and detection is all performed on PIC.

High precision ranging equipment is included for measuring the relative position and orientation of each spacecraft within the constellation. The three-dimensional arrangement of the constellation allows each vehicle to use a laser ranging system to solve for its position in space, and an inertial proof mass is used to measure constellation rotation.

When knowledge of the optical field amplitude and phase is combined with precise knowledge of sampling time and position, well-established radio astronomy techniques can be used to back out information about the source.[14] Increasing the number of spacecraft in the constellation, *n*, has the effect of increasing the number of baselines to $B = (n^2 - n)/2$, each of which corresponds to a sample in the u-v plane, while changing the length of each baseline changes the spatial frequencies to which the constellation is sensitive.

SRSAII stores all collected information locally on each spacecraft and all calculations are done in post-processing on the ground. Photon counting detectors that store data proportional to the number of photons collected, rather than the Nyquist rate for each channel, are implemented for improved sensitivity and significantly decreased data volumes. Final data volumes are anticipated to be on the order of tens of Gb/s rather than hundreds of Tb/s exhibited with a traditional detection scheme with similar optical bandwidth.

4. Conceptual Foundations for Interferometry

This section describes several important concepts as they relate to optical interferometry. Included are descriptions of first and second order optical coherence, the Van Cittert-Zernike theorem used to relate coherence to properties of the optical source. Also included are a description of the u-v plane as it relates to interferometry, the visibility function, and the rationale for extrapolation of classical interferometric techniques and concepts into the single photon regime.

4.1. Phase Correlation

Coherence is the most fundamental and important property of light as it pertains to interferometry. Two forms of optical coherence, temporal and spatial, exist and can be treated independently from one another to first order.

Temporal coherence is a property which appears when considering a light source with finite bandwidth, or frequency content. This property becomes most apparent through observation of two waveforms with slightly different frequencies, for instance from the opposite sides of an optical band-pass filter or a laser's linewidth, that interact at a single point such as an optical detector. As shown in **Figure 10**, the temporal location of the peaks of the two sinusoids drift relative to one another. Initially, the waves peak at the same time and are said to be coherent. As time progresses, however, the difference in their frequency means that the coherence of the waves, or alternatively, the correlation of their peaks, diminishes with time.

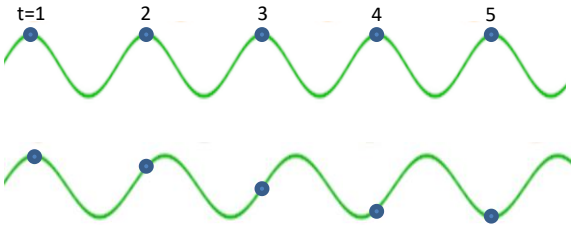

Figure 10: Illustration of the growing phase difference between monochromatic waves of different frequency. For a passband of width BW, the summed signals across the band lose coherence after a time interval of approximately 1/BW

By time 3, the waves have decohered enough that it is impossible for an outside observer to tell whether the measurement of the bottom sinusoid is lagging or leading the top sinusoid and the system is said to be degenerate due to two valid mathematical solutions for the measurement. The time for this degeneracy to occur can be thought of as the coherence time of the light. In a real system, the coherence time, t_c, is related to the optical bandwidth, $\Delta\nu$, by the simple relation: $t_c = 1/\Delta\nu$. This equivalency of the coherence time and the inverse optical bandwidth presents sufficient insight into temporal coherence of the field for a conceptual discussion, and all other necessary coherence properties follow from the descriptions below.

Spatial coherence quantifies the degree to which measurements of the phase fronts of the electric field at a reference plane correlate to one another across different degrees of separation, or baselines. Any real measurement is intrinsically a time averaged value resulting from the non-zero integration time of a detector, so the correlation itself is presented as a time-averaged value.

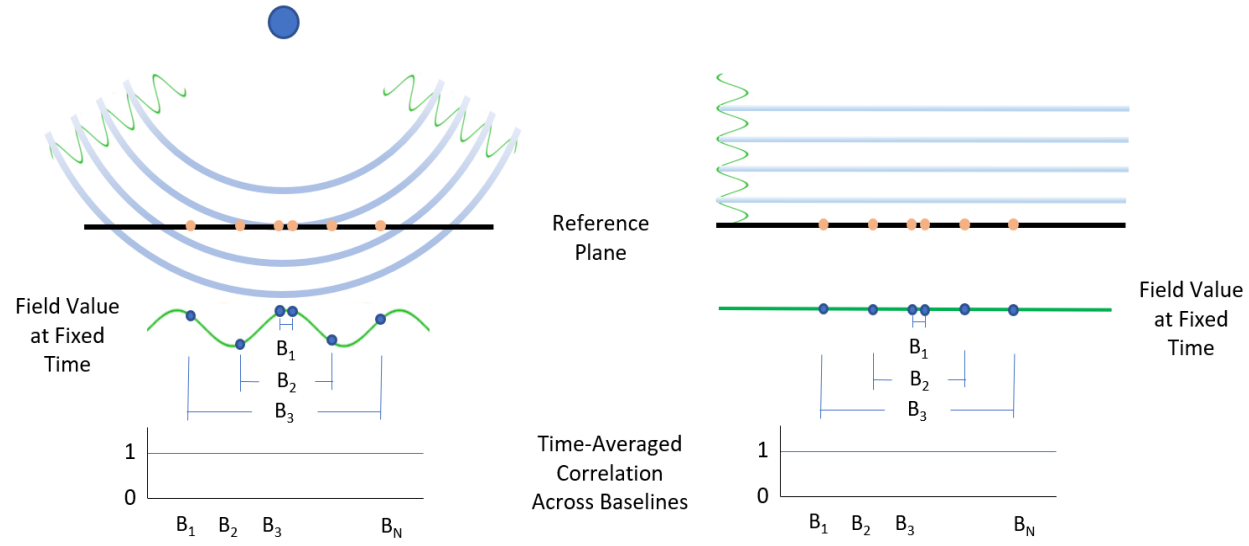

Figure 11: For a point source, the spatial coherence is infinite. In a measurement plane perpendicular to the source direction, the received signal is the same everywhere (in the limit of a very large distance to the source).

The phase fronts of a field emanating from a point source form concentric rings which expand radially outward in all directions as shown at left in **Figure 11**. When the electric field is measured at a reference plane, its different values can be related to one another, and the correlation as a function of baseline can be constructed. For real astronomical distances, these far-field phase fronts can be represented as plane waves (Figure 11, right), and for a true point source, the correlation function is unity for all baselines because the phase fronts arrive at each measurement point undisturbed. The simplest case where non-trivial information can be gathered is that of a pair of point sources, shown in **Figure 12**.

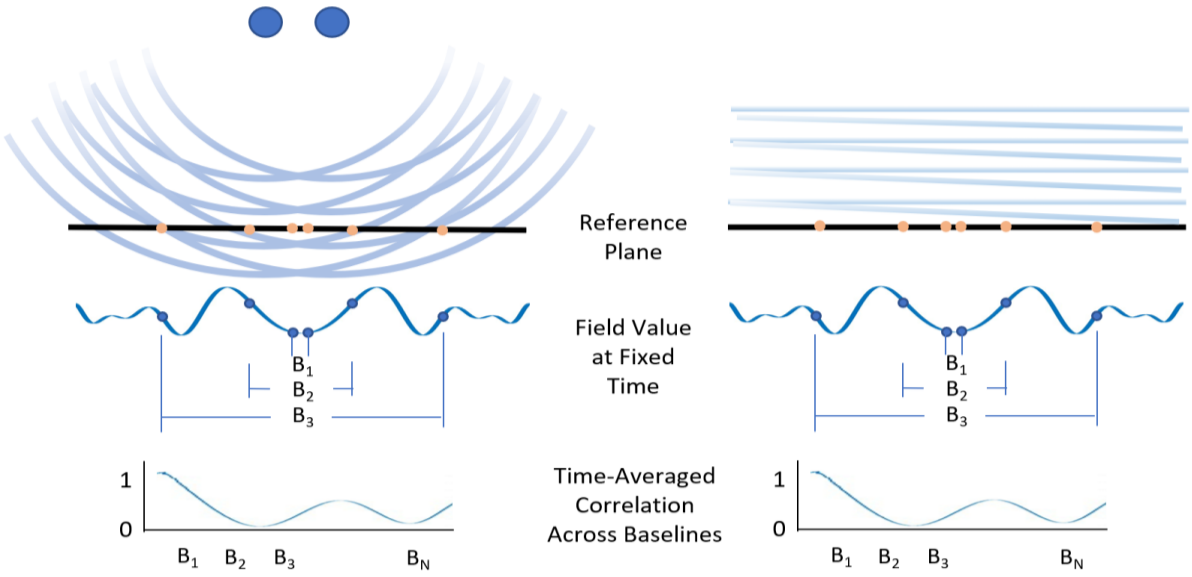

Figure 12: For a source consisting of two point emitters, the relative phase of light from the two points varies across the reference plane. Therefore, the cross-correlation function oscillates from one to zero with position on the plane. For a more realistic case where the two emitters have nonzero angular size, the cross correlation decreases in magnitude as the baseline increases.

The simplest case which yields non-trivial results is that of a pair of point sources, shown in **Figure 12.** The measurement in this situation is that of the total optical field, which is the linear superposition of the spherical fields emanating from each point source. Varying the measurement baselines reveals a pattern resulting from the constructive and destructive interference of the two fields. As with a single point source, both fields take the form of plane waves in the far-field, but a phase delay occurs from one field to the other due to the difference in the optical path from the source to the detector.

While the above descriptions of optical coherence are helpful for qualitative discussion and general conceptualization of interferometry, a rigorous mathematical treatment is necessary for complete understanding. The temporal and spatial coherence described above are examples of the first order phase coherence which are quantified by the normalized correlation function described below.

As any measurement is a time average of the measured value over the detector's integration time, the finite temporal coherence of the measured light means that the measurement coherence will decrease for increasing integration times. Correlation of the measured optical fields at two space-time points $(\boldsymbol{r}_1, t_1)$ and $(\boldsymbol{r}_2, t_2)$ is carried out for every period t_{int}, and is described by the correlation function.[15]

$$\langle E^*(\boldsymbol{r}_1, t_1) E(\boldsymbol{r}_2, t_2) \rangle = \frac{1}{t_{int}} \int_0^{t_{int}} E^*(\boldsymbol{r}_1, t_1) E(\boldsymbol{r}_2, t_1 + t_{21}) dt_1 \tag{2}$$

$$t_{21} = t_2 - t_1 \tag{3}$$

The optical field is the superposition of all optical field modes present at $(\boldsymbol{r}_1, t_1)$, such that

$$E(\boldsymbol{r}_n, t_n) = E_1(t) + E_2(t) + \cdots + E_m(t) \tag{4}$$

and is represented as

$$E(\boldsymbol{r}_n, t_n) = E_n e^{-i(\boldsymbol{k_n}\cdot\boldsymbol{r_n}+\omega_n t_n+\phi_n)}. \tag{5}$$

$E^*(\boldsymbol{r}_n t_n)$ is its complex conjugate, the $\langle\,\rangle$ brackets represent a time average, t_{int} is the integration time over which the average is taken, and $t_{21}$is the time delay between the arrival times of the correlated fields at each point. Traditionally, it is impossible to perform this correlation on white light within a single coherence time, so $t_{int} \gg t_c$. In the SRSAII system, limitation of the integration time to less than the coherence time, i.e. $t_{int} < t_c$, maximizes the temporal coherence of the two fields, greatly improving information retrieval capabilities.

Normalization of the correlation function gives a parameter, $g^{(1)}$, which is a quantification of the degree of first order (phase) correlation as a function of both space and time that is valid between 0 and 1. Measuring $g^{(1)}$ for varied time at fixed location gives a measure of the temporal coherence of the light, while measurement at fixed time for varied spatial coordinates, or baselines, reveals the degree of spatial coherence, which is the primary property that allows construction of an image of the source.[15]

$$g^{(1)}(\boldsymbol{r}_1 t_1, \boldsymbol{r}_2 t_2) = \frac{\langle E^*(\boldsymbol{r}_1 t_1) E(\boldsymbol{r}_2 t_2)\rangle}{\sqrt{\langle |E(\boldsymbol{r}_1 t_1)|^2\rangle \langle |E(\boldsymbol{r}_2 t_2)|^2\rangle}} \tag{6}$$

Where magnitudes of $g^{(1)}$ mean that the measured fields are:

$$g^{(1)}(\boldsymbol{r}_1 t_1, \boldsymbol{r}_2 t_2) \begin{cases} = 1 & \text{Completely Coherent} \\ < 1 & \text{Partially Coherent} \\ = 0 & \text{Incoherent Superposition} \end{cases}$$

For the case of interferometry, the sampled light must necessarily be in the partially coherent regime for meaningful information to be gathered. Completely coherent light can only come from a non-physical monochromatic point source, and entirely incoherent light has lost all information about its source.

4.2. Intensity Correlation

When gathering information about the source of an optical field, it is most typical to measure $g^{(1)}$ directly. It is not, however, the only means to come by this information. The second order correlation, $g^{(2)}$, can be measured with the second order electric-field correlation function:[15]

$$g^{(2)}(\boldsymbol{r}_1 t_1, \boldsymbol{r}_2 t_2; \boldsymbol{r}_2 t_2, \boldsymbol{r}_1 t_1) = \frac{\langle E^*(\boldsymbol{r}_1 t_1) E^*(\boldsymbol{r}_2 t_2) E(\boldsymbol{r}_2 t_2) E(\boldsymbol{r}_1 t_1)\rangle}{\langle E^*(\boldsymbol{r}_1 t_1) E(\boldsymbol{r}_1 t_1)\rangle \langle E^*(\boldsymbol{r}_2 t_2) E(\boldsymbol{r}_2 t_2)\rangle} \tag{7}$$

and related to $g^{(1)}$ through the relationship:

$$g^{(2)}(\tau) = 1 + \left|g^{(1)}(\tau)\right|^2 \tag{8}$$

Noting that $\langle I \rangle = \langle E^* E \rangle$, we can re-write $g^{(2)}$ in terms of intensity, which is a directly measurable quantity.[15]

$$g^{(2)}(\boldsymbol{r}_1 t_1, \boldsymbol{r}_2 t_2; \boldsymbol{r}_2 t_2, \boldsymbol{r}_1 t_1) = \frac{\langle I(\boldsymbol{r}_1 t_1) I(\boldsymbol{r}_2 t_2)\rangle}{\langle I(\boldsymbol{r}_1 t_1)\rangle \langle I(\boldsymbol{r}_2 t_2)\rangle} \tag{9}$$

While these intensity correlations are a fundamental property of light from a thermal or otherwise stochastic source, building a conceptual picture of the cause of the correlations, and their meaning, can be challenging.

Understanding $g^{(2)}$ is most easily done in the time domain, where it can be measured with a single fast photodetector, so the relative position vector falls out of the analysis. The behavior described by the equation below describes the correlation of field intensity between time t and a short time, τ, later and normalized to the average intensity at the detector.[15]

$$g^{(2)}(\tau) = \frac{\langle E^*(t) E^*(t+\tau) E(t+\tau) E(t)\rangle}{\langle E^*(t) E(t)\rangle^2} = \frac{\langle I(t) I(t+\tau)\rangle}{\langle I(t)\rangle \langle I(t+\tau)\rangle} \tag{10}$$

For a perfectly uniform optical field, i.e. one that is temporally coherent, $g^{(2)}$ is zero because the field intensity is uniform across all time. For a stochastic field, however, careful observation reveals that measurements of the field intensity tend to arrive in bunches with a characteristic width on the order of the field coherence time. **Figure 13** shows the behavior of light from a coherent source compared with light from a thermal source of equal intensity.

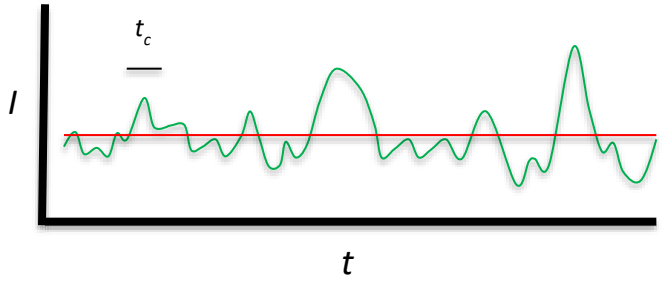

Figure 13: Illustration of the 'bunching' in photon arrival times due to nonzero $g^{(2)}$. The red line represents a coherent field, and the green line represents a stochastic field

To understand this bunching effect, it is helpful to consider a simple model of the thermal source as a collection of emitters that generate optical fields of the same wavelength, but arbitrary phase. The net field emitted from this collection can be written as:

$$E_{net} = \sum_n E_n e^{-i(\omega t + \phi_n)} \tag{11}$$

When two of the emitters collide, they resettle into a new steady state where each has the same wavelength and amplitude as before the collision, but a newly randomized phase value, ϕ (**Figure 14**). This changes the amplitude of the net electric field as it propagates away from the source.

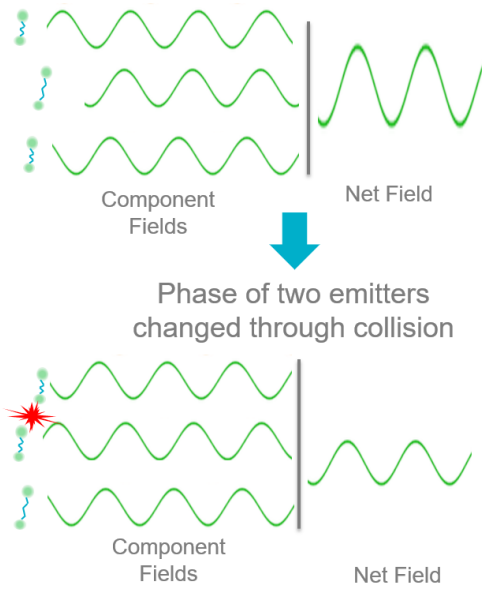

Figure 14: Change in the net emitted electric field in a thermal source.

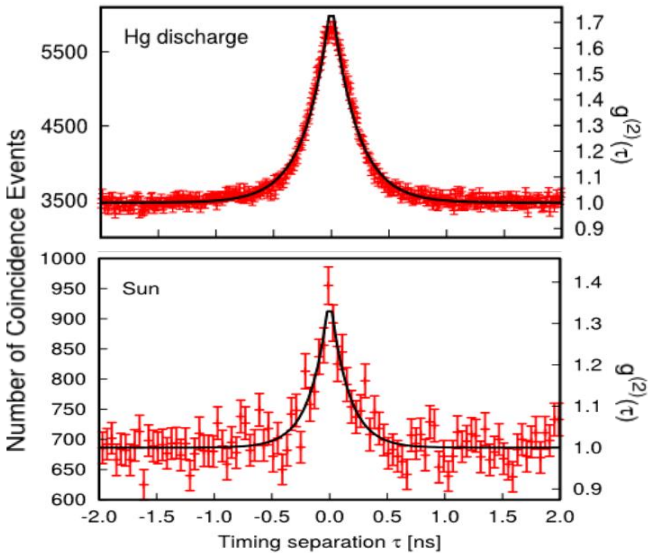

Figure 15: Measured temporal photon bunching in thermal emission from a mercury discharge lamp (top) and the Sun (bottom).[16]

Real-world measurements of $g^{(2)}$ as a function of time (**Figure 15**) reveal that a field's intensity correlates with itself over a time related to its coherence time. The measurements below, taken by Tan et al, show the $g^{(2)}$ correlation for real white light filtered to have $t_c \approx 0.25ns$. As can be clearly seen, there is significant bunching about $\tau = 0$, representing the increased probability for continued high field intensity for a short duration after detection of a high intensity pulse.

While the above classical analyses and logic hold even for very low light levels, it is also valuable to consider the case where field amplitudes are low enough that individual photons are detected. In this case, the $g^{(2)}$ parameter represents the likelihood of detection of a second photon within a coherence time of the detection of a first.[17] As shown in **Figure 16**. For thermal sources (bottom), a distinct "bunching" effect can be seen when compared to a 1st order coherent source (top), such as a laser, where photon arrival times show no bunching and are governed by Poisson statistics.

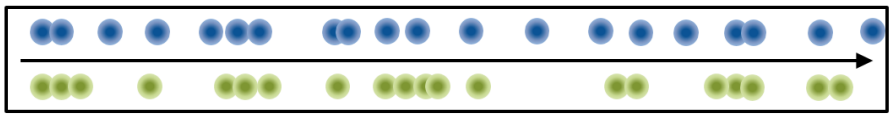

Figure 16: Photon arrival times from a coherent laser (top) with no bunching, and a thermal source (bottom) with bunching.

4.3. Van Cittert-Zernike Theorem

The Van Cittert-Zernike states that the complex degree of correlation, $g^{(1)}$, of the optical field generated by an incoherent, extended, quasi-monochromatic source creates the same pattern as the diffraction of a spherical wave through an aperture of the same size and shape of the source.[18]

A rigorous discussion of this theorem is beyond the scope of this report, but the relevant implication is that for a far-field source that is located such that both the characteristic dimension of the source and maximum observing baseline are very small in comparison to the distance between the source and observer, the pattern created by $g^{(1)}$ is equal to the absolute value of the normalized Fourier transform of the intensity function of the source.

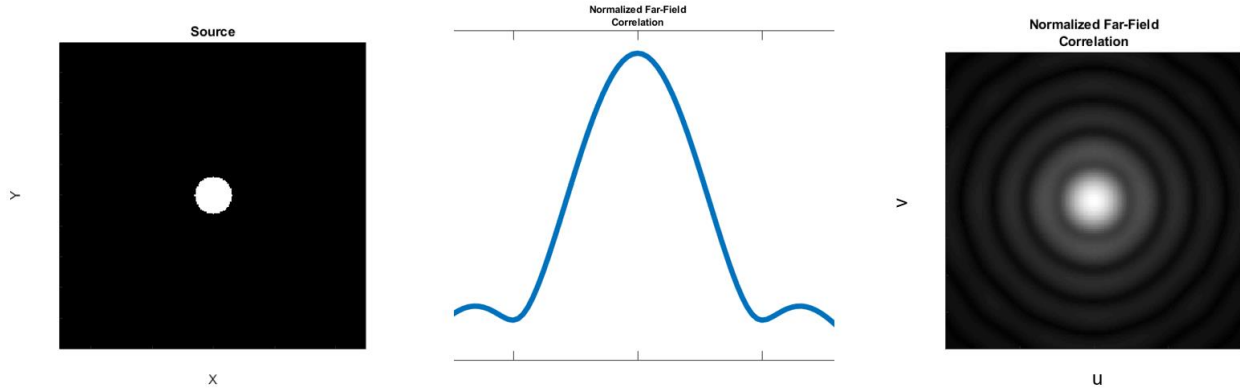

Figure 17: Illustration of the Van Cittert-Zernicke theorem, in which the far field coherence pattern corresponds to the Fourier Transform of the source brightness distribution.

This means that mapping $g^{(1)}$ as a function of baseline reveals the Fourier transform of the source (see **Figure 17**). Measurement of $g^{(1)}$ can either be made directly or through higher order correlations such as $g^{(2)}$, and many methods exist to reconstruct information on the source from the $g^{(1)}$ distribution.[17,19]

4.4. u-v plane

Although a spacecraft constellation is most easily visualized by their relative position in free space, the key parameter for a sparse-aperture interferometer is the distance and orientation of the baseline between each sub-aperture pair.

As described by the Van Cittert-Zernike theorem in Section 4.3, the degree of first order correlation of the optical field between two points in space represents the amplitude of the spatial Fourier Transform of the field's source at the spatial frequency represented by the mapping of the baseline into the Fourier Plane, (u,v). This mapping becomes clear when each baseline is defined as a vector $\boldsymbol{B} = (B_x, B_y, B_z)$. Representation in Fourier coordinates follows as $u = \frac{B_x}{\lambda}$ and $v = \frac{B_y}{\lambda}$. The component B_z does not affect the measured visibility, but in practice, this component is minimized to eliminate losses resulting from the finite coherence time of the sampled light. Despite efforts to minimize B_z, residuals exist in any real system, and the measured signal phase experiences a time delay of $\tau = \frac{B_z}{c}$. This time delay affects any interferometer, and analog systems such as direct detection are required to actively compensate in real time, subtracting out nanometer-scale values of B_z in real time using exquisite optomechanical controls. One of the greatest benefits of a digital system is that these time delays can be removed in post-processing, requiring knowledge of the location of each sub-aperture relative to the constellation, but not necessitating their control to sub-wavelength levels.

The distribution of the correlation, represented by the visibility function, V, as a function of the angular distribution of the source on the sky is most concisely represented by the Fourier Transform pair:[20]

$$V(u,v) = \iint I(\xi,\eta) e^{2\pi i(u\xi+v\eta)}\, d\xi d\eta \tag{12}$$

$$I(\xi,\eta) = \iint V(u,v) e^{2\pi i(u\xi+v\eta)} du dv \tag{13}$$

In the above equation, the brightness distribution $I(\xi,\eta)$ has been normalized such that the integral over the entire sky is unity. $V(u,v)$ is the visibility function, which is unity for an unresolved point source, and has a magnitude less than unity for any real source.

Using a system which can measure optical correlation at many baselines allows the construction of the (u,v) plane as the set of discrete points:

$$(u,v) = \left(\frac{B_x}{\lambda}, \frac{B_y}{\lambda}\right) \tag{14}$$

In the ideal case, a continuous array of such points is constructed, with one baseline per point, and the inverse Fourier Transform reveals an image of the source with maximum resolution:

$$(\delta\xi, \delta\eta) \approx \left(\frac{\lambda}{B_x(max)}, \frac{\lambda}{B_y(max)}\right) \tag{15}$$

The fidelity of the image is directly related to the completeness of the (u,v) plane sampling. For an ideal system such as a diffraction-limited telescope with a continuous aperture, an infinite number of baselines exist and the (u,v) plane is completely sampled across the full collecting optic. The resulting images are therefore continuous and free of diffraction effects related to sparse apertures. For systems where most of the (u,v) plane has been sampled, but some holes exist, the spatial frequencies in the source profile that correspond to each of the holes will not be represented in the final images. This results in blurring or loss of certain features in the images.

Sparse apertures, where the (u,v) plane is sampled only at a few baselines result in a limited number of spatial frequencies being represented in the final image.

Rotation of the entire constellation allows each baseline to sample a curve through the (u,v) plane, greatly increasing fidelity of the resulting image. This is typically done with radio telescopes, often by taking advantage of the natural rotation of the earth with respect to the astronomical source. A free-flying constellation such as SRSAII will allow mission designers to search astronomical targets for spatial frequencies of interest, and the digital nature of the data allows maximization of the number of baselines without incurring losses associated with beam combination. Significant research into computational methods for reconstructing sources sampled with sparse apertures is ongoing, and similarity of the data output by SRSAII to that of radio telescopes will allow leverage of a large volume work in fields such as computational imaging.[14,21,22]

4.5. Visibility Function

Fringe visibility is a key concept for understanding the function and limitations of an interferometer. The simplest picture of an interferometric fringe is that observed when an ideal Michelson interferometer is scanned over several longitudinal modes. For the ideal normalized case, shown in **Figure 18**, the detected intensity, which is directly related to $g^{(1)}$, as shown in **Equation 8,** varies from zero to unity and calculation of the visibility function reveals $V = 1$.

$$V = \frac{I_{max} - I_{min}}{I_{max} + I_{min}} \tag{16}$$

For cases where fringe contrast is reduced, perhaps because the 50:50 split in a Michelson interferometer is less than ideal, or detection of stray light in the interferometer results in an intensity offset for the fringe pattern, visibility is less than unity.

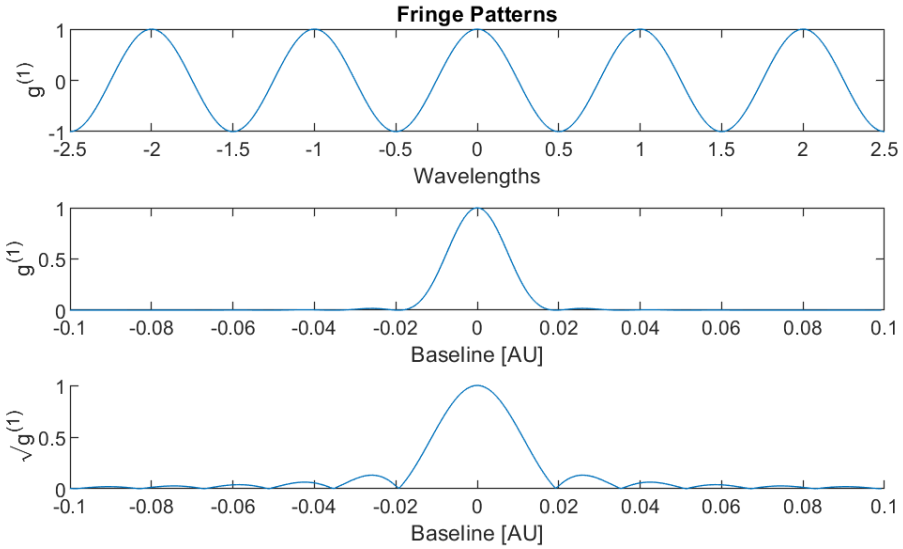

Figure 18: Top. Fringe pattern for a Michelson interferometer for a source consisting of two point emitters. Middle. Fringe pattern for a uniform disk source. Bottom: Square root of middle plot to show the secondary peaks.

In the case of the astronomical interferometer (middle, Figure 18), variations in detected intensity due to $g^{(1)}$ are only observed for direct detect, where the beams are combined in the same manner as the Michelson. Heterodyne and intensity interferometry calculate $g^{(1)}$ by cross-correlating signals in post-processing. As shown in the bottom plot in Figure 18, the magnitude of the visibility decreases greatly with increasing baseline.

4.6. Low Light Limit

In the low light limit, instead of considering intensity detection as a field fluctuation, we consider the light field to represent a probabilistic distribution of photons in time. Thus, a photon detector measures photon arrival events corresponding to this probabilistic distribution, with

proportionality constant related to either detector responsivity or quantum efficiency depending on the detector.

Figure 19: For the low light limit, treatment of light as a classical wave breaks down, but instead is observed as a set of photon arrival times.

The modal characteristics (spatial distribution) we can ignore for the implementation of SRSAII. Several authors have presented expositions on this subject[23,24] which we will summarize here. Following the convention of Liu et al, we will write here a few expressions that may aid in the understanding of this probabilistic picture.
Probability of detection of one photon in some interval δt is proportional to the intensity, but the integral expression alludes to the Poissonian behavior of these photon events.

$$P(t-\Delta t,t)=\eta\int_{t-\Delta t}^{t}I(t')dt'\exp\left[-\eta\int_{t-\Delta t}^{t}I(t'')dt''\right]\approx\eta I(t)\Delta t \tag{17}$$

With *I(t)* representing the field intensity in time, and η the photon detection efficiency of the detector. If one were to assume the intensity I(t) constant in time, the expression for the probability density over some time interval τ is simply the Poisson distribution with expected value N.

$$P(\tau)=Ne^{-N\tau} \tag{18}$$

Where N is the expected count rate $N=\eta I(t)$.

This convention holds for both direct observation of the low light field and homodyne and heterodyne techniques. The interference of fields in heterodyne detection happens classically, and the quantization of the interfered field (amplitude, frequency, and phase) happens at the detector.[25, 26, 27] As a result, the detected heterodyne signal analogously takes on a probabilistic distribution in time proportional to the interfered fields.

The presented references show some examples of this for practical applications. Winzer [25] considered the low light level coherent detection problem for Doppler lidar. When considering classical light, you can treat the electromagnetic field classically, and only at detection consider the discrete nature of light (quantization). In the detector, photons are converted to electrons with some quantum efficiency η. Therefore, simplistically, the statistics of the generated electrons exactly mimic the statistics of the photons. As the photon distribution can be considered as manifested by the intensity distribution (the observable), one can then conclude that the photoelectrons are thus proportional to the intensity (as a function of space and time). This may seem obvious, but we must remember that the descriptor of photoelectrons is to be considered as a probability distribution of discrete events (detected photons).

Even in the low photon regime, a heterodyne beat between a weak signal and a stronger LO is detected by a photodetector that sees the beat field but yields a photoelectron distribution corresponding to the probability distribution of photons, wherein the probability distribution is proportional to the beat amplitude. To answer the question of what SNR should we expect of a "few photon" heterodyne detection system, we only have to look to the semi-classical understanding of heterodyne mixing and understand that the photoelectron distribution is proportional to the expected beat intensity.

Now, returning to the mathematical formalism, one can write the heterodyne intensity from our semi-classical understanding

$$I_{beat}(t) = I_{LO} + I_S + 2m\sqrt{I_{LO}I_S}\cos(\omega_{IF}t + \varphi) \tag{19}$$

and interject the corresponding probability representations for I_S and I_{LO}, arriving at the picture of photon arrival times corresponding to the beat signal power (fig 1 of Liu, or Kovalyuk fig 1(d)(e)). The precise expression can be found in equation (13) of Liu et al, but here we point out the functional dependence $p_{beat}(t) = f\left(N_S, N_{LO}, T, \omega_{IF}, \tau, \varphi, t\right)$. Liu then goes on to compare this probability distribution of the beat signal with the dark photon distribution, which also follows a Poissonian distribution.

Further confirmation of this understanding of the low light detection regime can be found in descriptions of classical and quantum communications. Shapiro presents a detailed review of signal detection for direct (un-mixed), homodyne, and heterodyne detection schemes[22]. He shows that in the case of detecting classical light (true in our case), the semi-classical and quantum approaches converge, even in the low light limit. In light of this conclusion, the quantum derivation will not be summarized here.

4.7. Types of Optical Interferometry

Several kinds of optical interferometry exist, and four are described below. Direct detect, also known as homodyne, is included primarily for comparative purposes. The purpose of the SRSAII study is to evaluate alternatives to this method, as implementation has proven to be a significant challenge for even small numbers of modest baselines. The heterodyne interferometry technique presented below is the most promising approach for near term optical observation of astronomical targets with very long baselines. Intensity interferometry and quantum-assisted interferometry are techniques that show promise and were studied in SRSAII. A description of each technique, along with benefits and weaknesses are described below.

4.7.1. Direct Detection

Direct detection, or homodyne, interferometry is the most natural extension from a traditional telescope. A direct detection interferometer can be created by masking portions of a primary optic or, in the case of a segmented optic, only implementing certain segments (see **Figure 20**). Because the fundamental purpose of an imaging system is to provide information on the $g^{(1)}$ optical correlation, it is unnecessary for collecting optics to be restricted to a traditional structural

arrangement. In fact, optical assemblies can be designed to carry out this task with each collecting assembly physically separated from the detector.

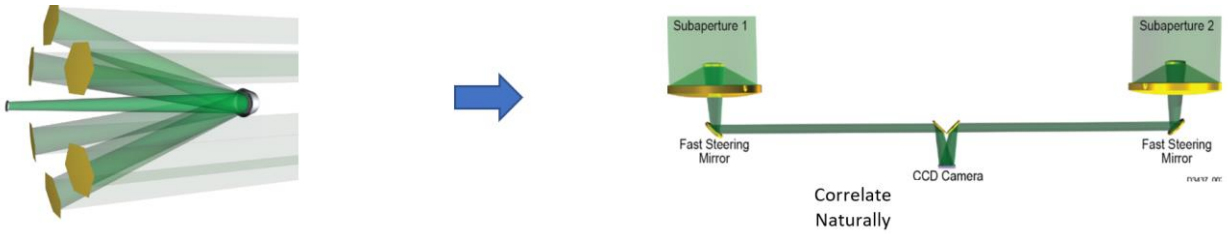

Figure 20: Illustration of the light and detection path for direct detection interferometry. Light from the two telescopes is brought together for detection in real time.

Because this technique is phase sensitive, however, the opto-mechanical requirements dictate that the relative optical path from each collecting optic to the detector be controlled to much less than a wavelength. In practice, systems employing this technique often rely on complex systems to control delays in real time and combine optical beams onto a detector.

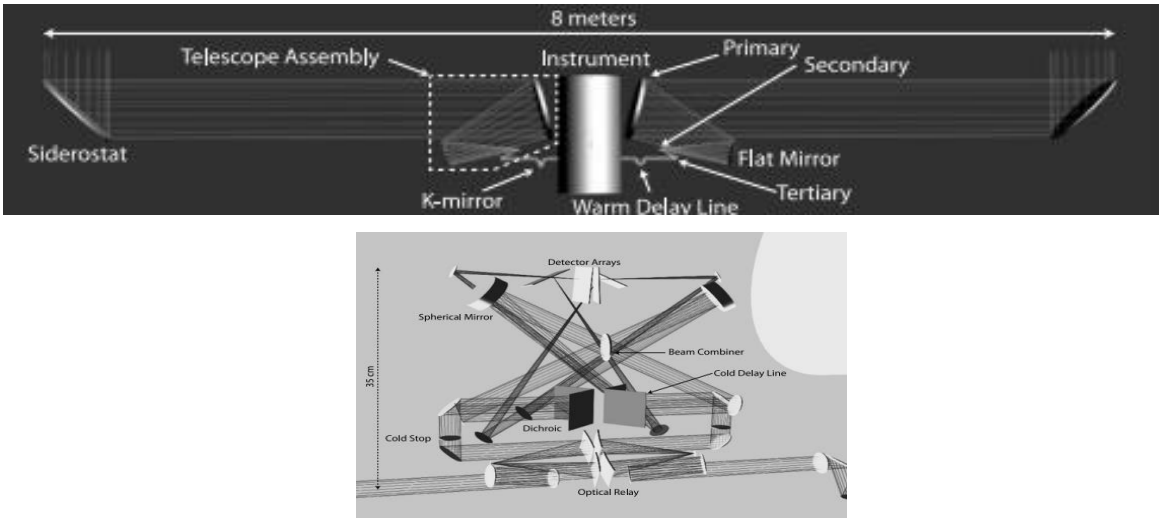

Figure 21: Schematic of a real-world direct detection interferometer, BETTII, operating in the mid-wave infrared. A complicated optical system is required for direct detection interferometry. Top: Full scale layout including collecting sub-apertures (siderostats). Bottom: Cooled optical system inside cryogenic assembly.[9]

The system shown in **Figure 21**, known as BETTII, operated in the mid-wave infrared and combined two beams collected across a baseline of 8 meters.[9] The figure is included to demonstrate the complexity of real-world implementation of a single baseline for direct detection. Adding baselines or extending the one already constructed would have significantly increased system complexity and may have led to diminished SNR due mechanical tolerances and beam propagation effects.

Despite the many technical challenges that face direct detection interferometry, it is the preferred configuration for observing dim targets due to its relatively high shot-noise limited SNR.[5]

$$SNR = V_{nm}\sqrt{rT_{obs}} \tag{20}$$

In this familiar picture for the amplitude SNR of a direct detection system, V_{nm} is the visibility across the baseline between spatial coordinates n and m, T_{obs} is the observation period, $r = \frac{\eta P}{h\nu}\Delta\nu_{total}$ is the detected photon flux in photons/sec. Note that for this analysis, the spectral bandwidth, $\Delta\nu$, is assumed to be 20%, and system efficiency, η, is assumed to be unity. For a ground-based system, T_{obs} is limited to the atmospheric coherence time, however a space-based system can extend observation times until the next limiting system factor is reached. For a system with sufficient stability and positional control, T_{obs} could potentially be extended to hours or even days.

$$T_{obs} = \frac{SNR^2}{(V_{nm})^2 r} \tag{21}$$

The primary benefit to direct detection interferometry is the sensitivity of the technique to the first power of the visibility function and the *square root* of the number of detected photons.[5] This becomes especially critical for dim targets, where the required observation time for a meaningful SNR is proportional to the number of detected photons, rather than the *square* of the number of detected photons, as is the case for heterodyne interferometry.

The primary challenges to this technique are related to the physical combination of the light collected at each source. Furthermore, opto-mechanical design complexity limits most direct detection interferometers to a few baselines at most.[9]

4.7.2. Intensity Interferometry

Originally described as a "new type of stellar interferometer" by its creators, Hanbury Brown and Twiss recognized that measurement of the arrival *time* rather than phase of photons could be used to measure the second order optical correlation function of light from a stellar source. Due to the fact that this technique does not involve interfering optical signals, the term intensity interferometry is actually a slight misnomer.

The basic architecture for an intensity interferometer involves an optical detector at each aperture and a method to cross-correlate their time series. This can be done with analog detectors, combining the time series data in a mixer and varying an electronic delay in real-time, δ, to find the maximum degree of correlation for a given baseline. Alternatively, modern detection schemes allow the data to be digitized and cross-correlated in post-processing, eliminating the need for a physical connection between detectors.

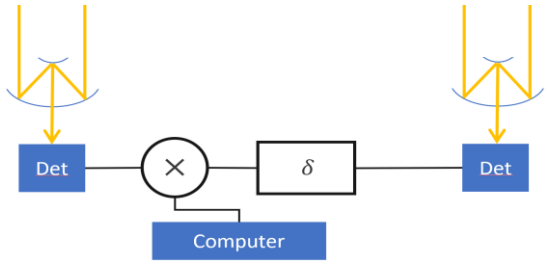

Figure 22: Schematic for an intensity interferometer. Light is collected at each telescope and cross-correlated in a computer.

The degree of second order correlation obtained across any given baseline represents a magnitude of the visibility function at point in the (u,v) plane. From this measurement, the straightforward relation between $g^{(2)}$ and $g^{(1)}$ allows use of the Van Cittert-Zernike theorem to calculate the structure of the source. The formulation below differs from that in section 4.2 in that it has been expanded from a purely temporal correlation to one in space-time where $X = (x, y, z, t)$.

$$g^{(2)}(X) = 1 + \left|g^{(1)}(X)\right|^2 \tag{22}$$

There are several benefits to employing the intensity interferometry method. Notably, because the features measured by this technique have a characteristic time on the order of the coherence time of the sampled light, it is not necessary to implement a complex LO scheme to measure optical phase, and error on the order of hundreds of picoseconds can easily be tolerated without degrading performance. This corresponds to many centimeters of optical path, greatly reducing requirements for optical path control when compared to a telescope or direct-detect interferometer.

Due to the lack of phase sensitivity, intensity interferometers are not required to form clean images with each optic, so it is unnecessary for ground-based systems to implement adaptive optics to counteract atmospheric effects or use diffraction limited optical assemblies. In fact, for the original demonstration by Hanbury Brown and Twiss, "the two mirrors were the reflectors of two standard search lights".[28] It is precisely these characteristics of intensity interferometry that allowed the angular diameter of Sirius to be resolved with this method as early as 1956.

While the loose requirements on optical delay decreases the optical design requirements for a system, it means that a two-detector intensity interferometer is insensitive to the structure phase of the target, only providing information about the target silhouette. Addition of a third detector allows measurement of structure phase by means of the 3rd order intensity correlation, making it possible to detect structures such as starspots, but this technique significantly reduces SNR and is only useful for exceptionally bright targets.[29] In practice, third order intensity interferometry is unlikely to prove useful for any astronomical targets.

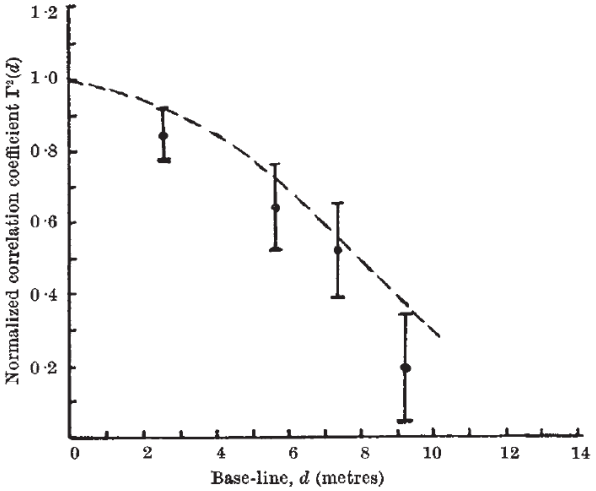

Figure 23: Measured visibility on Sirius, the brightest star in the sky, with values from a simple circular 'disk' model shown for comparison.[28]

Despite the success of the original experiments, this technique has seen limited use because its intrinsically low SNR renders it impractical for all but the brightest of targets. Advancements in detector technology have revived interest in this technique, however few significant advancements have occurred beyond increased detection efficiencies.

$$SNR = (V_{nm})^2 \, r\sqrt{T_{obs} t_c N} \tag{23}$$

As can be seen in the formulation above, SNR is a function of the visibility across the baseline from n to m, V_{nm}, squared, the photon detection rate for each channel, $r = \frac{\eta P}{h\nu}\Delta\nu_{channel}$, the optical coherence time for a given channel, t_c, observation time, T_{obs}, and the number of channels, *N*. This result can be seen explicitly in the work by Wentz and Saha, and the formulation seen in **Equation 23** is arrived at for detectors with sufficient temporal resolution to resolve the coherence time of a single channel.

Increasing the number of parallel channels, *N*, *does* improve the SNR by a factor of $\sqrt{N}$. While this has traditionally been impractical, the SRSAII system proposes to do just this, leveraging modern techniques to accomplish this on a photonic integrated circuit rather than a fiber or free space approach. Implementation of the SRSAII system for intensity interferometry results in an increase in SNR on order of 100, leading to a decrease in the required observation time to achieve SNR > 1 by a factor of 10^5 or more, depending on the number of channels utilized. This can be clearly seen when comparing the below formulation for observation time with a single channel traditional system to that with the SRSAII system with ~500,000 parallel channels. [2]

$$T_{obs} = \frac{SNR^2}{(V_{nm})^4 r^2 t_c N} \tag{24}$$

Figure 24 shows the performance of a single channel intensity interferometer compared with the multi-channel SRSAII configuration.[30] Using optics with a 1.5m radius, a 0.1 visibility can be resolved for a 10th magnitude object in less than a day. With the SRSAII multi-channel technique, it will be possible to resolve the diameters of objects far too dim to measure with a single channel system.

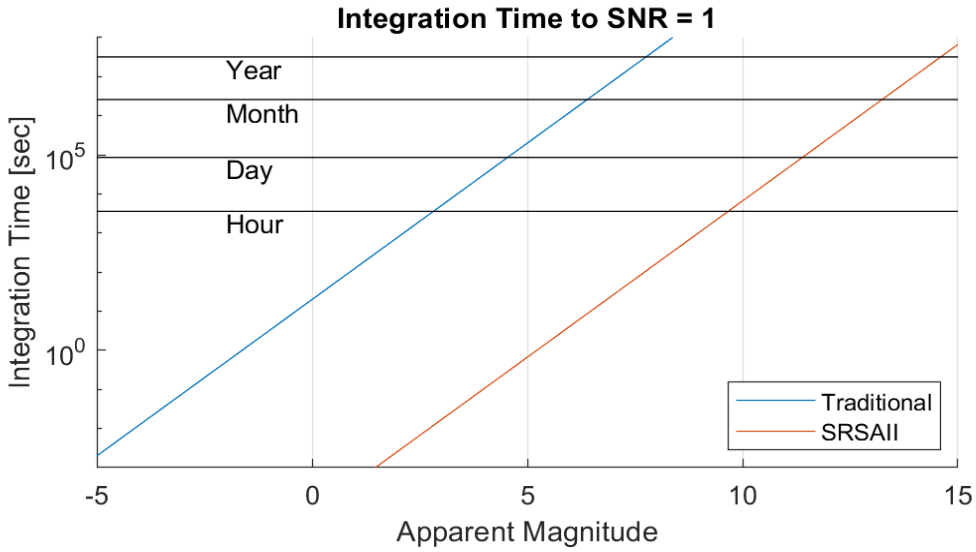

Figure 24: Required integration time for an intensity interferometer to achieve SNR = 1 with a baseline sampling a visibility of 0.1 with a 1.5m radius telescope. The distinction between traditional single channel (top) and SRSAII (bottom) is due to the number of parallel channels in the SRSAII system.

4.7.3. Heterodyne Interferometry

Heterodyne interferometry is the primary technique used by SRSAII. This technique, in which complex field information about the electric field is collected and measured at multiple points in space, is akin to the radio astronomy technique known as very long baseline interferometry. Despite operating in the optical domain, many of the post-processing techniques developed over decades of radio astronomy can be applied to data collected with SRSAII.

Data collection with a heterodyne interferometer is quite different from Direct Detection interferometry. In heterodyne interferometry, light collected by each sub-aperture is mixed with a stabilized reference laser known as a Local Oscillator (LO). When light from the astronomical target and the LO are combined and detected by a detector sensitive to optical field intensity, a heterodyne beat is formed. The amplitude and phase and timing of the optical signal collected from the astronomical target is converted into the radio frequency domain where it can be measured for each sub-aperture using commonly available electronics.

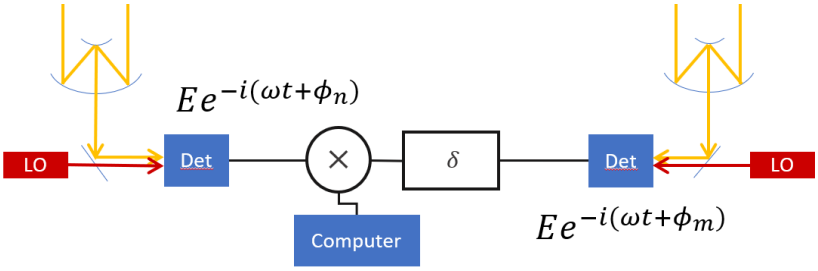

Figure 25: Schematic of heterodyne interferometry. Light from each telescope is mixed with a laser local oscillator, a relative delay is introduced between the two paths, and then digital cross correlation is performed.

Digitally combining this information with knowledge of the position of each sub-aperture allows comparison of the information gathered at each sub-aperture in post-processing rather than the real time combination and control of the optical field as is necessary when implementing direct detection interferometry. Furthermore, the nature of the correlating the collected signals in post processing allows cross-correlation between each of the $n = \frac{m(m-1)}{2}$ baselines in a constellation of m telescopes without suffering the $\sqrt{n-1}$ SNR loss factor associated with direct detection interferometers.

As shown by Ashcom the SNR for a heterodyne interferometer is governed by:[5]

$$SNR = V_{nm}\, r\sqrt{T_{obs} t_c N} \tag{25}$$

Where $r = \frac{\eta P}{h\nu}\Delta\nu_{channel}$ represents the photon count rate for each channel. This equation is derived using semi-classical arguments in Section 4.1, however as explained in Section 4.6, classical, semi-classical, and quantum mechanical arguments all converge to the formulation above despite operation in the single-photon regime. In modern radio telescopes, for instance, measurements are routinely built up from signals so weak that the mean time between photon

arrivals from the astronomical source at the detector is on the order of thousands of times the coherence time, or inverse of the bandwidth, of the signal.[31]

While this method suffers an SNR penalty of the square root of the collected photons when compared to imaging with a traditional telescope or direct detection interferometer[32], the significant decrease in complexity and digital combination of the signals gathered from each sub-aperture allow observation at many more baselines, and thus higher spatial fidelity, than beam combining methods. The SRSAII architecture offers a multi-channel approach to heterodyne interferometry which decreases required observation times for low-light measurements by a factor of 10^4 when compared to single channel heterodyne approaches. As is seen in the below formula for the observation time required to achieve a given SNR, SRSAII does not fully compensate for the lowering of SNR from that of a direct beam combination.

$$T_{obs} = \frac{SNR^2}{(V_{nm})^2 r^2 t_c N} \tag{26}$$

Even so, this novel technique promises a path toward sampling objects as deep as 15th magnitude with arbitrarily large baselines and mission flexibility that allows addition or subtraction of baselines as mission needs and resource availability dictate.

Figure 26 shows a comparison between anticipated required integration time for a traditional optical heterodyne interferometer and that for the SRSAII system. The primary reason for the significant increase in sensitivity for the SRSAII system is number of parallel channels. Utilization of PIC technology makes 500,000 channels realizable, and implementation of the ultra-precise photon counting detectors bring the data rates into a manageable range, likely on the order of tens of Gb/sec for the entire 500nm to 2000nm optical band.

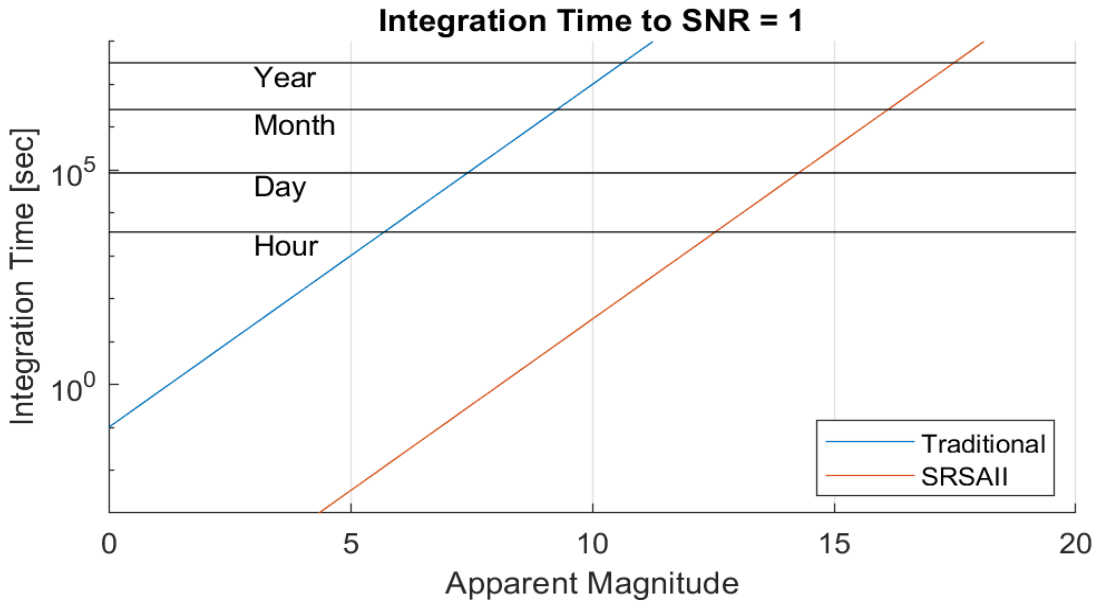

Figure 26: Required integration time for a heterodyne system to achieve SNR = 1 with a baseline sampling a visibility of 0.1 with a 1.5m radius telescope. The distinction between traditional (top) and SRSAII (bottom) is due to the large number of parallel channels in the SRSAII system.

4.7.4. Quantum Assisted Interferometry

The SRSAII team investigated the derivations of the SNR models for direct detect, heterodyne, and intensity interferometry all the way to first principles. This close inspection revealed that the decrease in SNR from direct detection to heterodyne interferometry – by a factor of the square root of the number of detected photons – is truly fundamental and cannot be overcome with any new configuration of classical measurements of the optical field.[33]

In the semi-classical picture, the fundamental distinction between heterodyne and direct detection interferometry is that one photon from the target source is sampled at *each* detector for a heterodyne system, and their information is then correlated. In contrast, a direct detection interferometer allows the optical field from the source to propagate along all possible paths in the optical system before sampling each photon on a detector. The patterns which the detector measures, therefore, are the fringes which result from the photon interfering with itself. This subtle but important distinction means that each measurement with a direct detection interferometer only removes one photon-equivalent of energy from the optical field, while the heterodyne interferometer removes two.

Measurement of the optical field with a classical system results in discrete information – two photons are coherent to a certain degree and not any others – and cannot overcome this fact. Use of a quantum system, however, should allow for an interferometer which does not have to combine optical beams but is also not limited by the two-photon problem described above. Several papers in recent literature [32,34],[35] have pointed to architectures based on the collection and storage of information about the optical field in quantum bits (q-bits) rather than classical binary bits.

Rigorous quantum formalism is used to describe the difference between the SNR of heterodyne interferometry and that of direct detection interferometry. [32,35] In the quantum picture, which is not described in this report, two distinct classes of measurement are defined: local and non-local.[32] In a local measurement, the class to which heterodyne interferometry belongs, the spatial coherence, $g^{(1)}$, is calculated from two local measurements – one at each end of the optical baseline. In a non-local measurement, such as direct detection interferometry, the two measured quantities are combined, resulting in the superposition of their quantum states. The final superposition of the two photons is measured directly, rather than the states of each of the individual photons. [32]

Fisher information is used to rigorously describe the amount of independent information which is obtainable from a measurement. This metric is a function of the quantum state of the measured system, typically defined in terms of a state-density matrix, and the specific measurement. The reader can find a detailed description of Fisher information in the paper by Tsang[32] the supplemental material provided by Khabiboulline.[33] Further detail regarding a quantum-assisted telescope array can be found in the literature,[34] where a quantum measurement and encoding scheme is described to allow a non-local measurement to be made. Such a configuration would exhibit many of the benefits of heterodyne interferometry like decreased mechanical complexity and greater baseline lengths and quantities compared to direct detect. Unlike heterodyne interferometry, however, a quantum-assisted measurement would have sensitivity similar to that

of direct detect. This type of system is likely the most approachable technique for multi-pixel resolution of exoplanet disks.

4.7.5. Technique Comparison

Comparison of the observation times for low visibilities shows a distinct disadvantage for intensity interferometry due to the proportionality of its SNR with the square of the visibility. This is the direct result of the technique's reliance on the second order correlation function, $g^{(2)}$. The other techniques are less affected as visibility decreases. A multi-channel heterodyne system as studied for SRSAII is able to resolve an 11th magnitude object with about a day of continuous observation. The clear winners from a purely SNR perspective, however, are the direct detection and quantum assisted interferometry techniques. They are plotted here on the same line as their difference in theoretical maximum sensitivity is not visible on this scale.

This comparison demonstrates the significant capability of a fully implemented direct detection or quantum assisted interferometer, but also points to multi-channel heterodyne interferometry as a techniqe that is sensitive to completely unexplored parameter space. The ability of SRSAII to measure visibility of V = 0.1 for targets out to 15th magnitude will allow precise spectral measurements to be combined with spatial resolution sufficient to determine diameter and aspect ratio of many thousands of unresolved astronomical targets. Measurement of visibility of V = 0.005 will allow scientists to begin to study surface features on targets out to 10th magnitude with integration times of only a few hours.

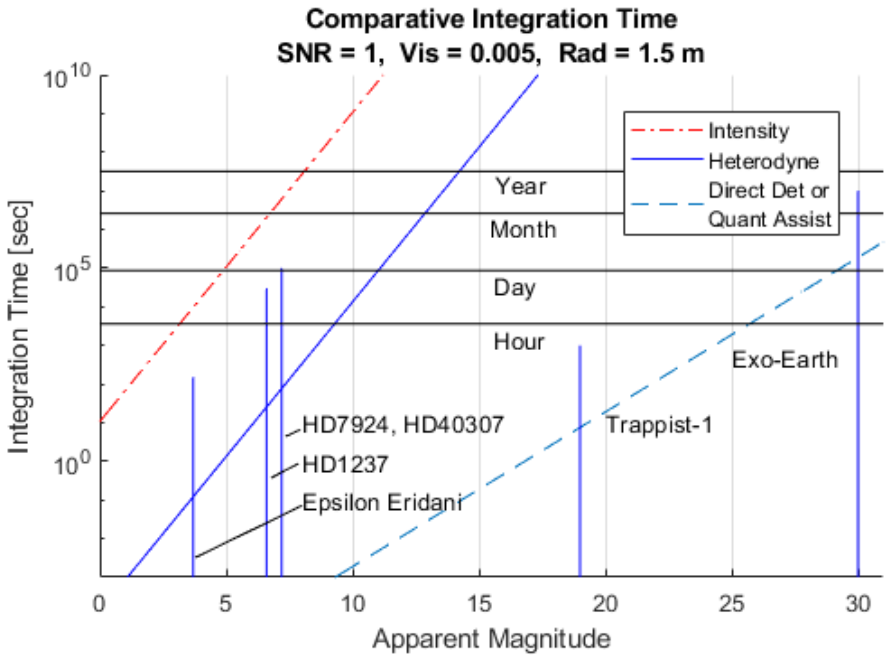

Figure 27: Sensitivity comparisons for the architectures considered in this study, for a 1.5 m radius telescope and an interferometric visibility

This comparison demonstrates the significant capability of a fully implemented direct detection or quantum assisted interferometer, but also points to multi-channel heterodyne interferometry as a techniqe that is sensitive to completely unexplored parameter space. The ability of SRSAII to measure visibility of V = 0.1 for targets out to 15th magnitude will allow precise spectral

measurements to be combined with spatial resolution sufficient to determine diameter and aspect ratio of many thousands of unresolved astronomical targets. Measurement of visibility of V = 0.005 will allow scientists to begin to study surface features on targets out to 10th magnitude with integration times of only a few hours.

5. SRSAII Detection Process and Techniques

Light collection is carried out for all spacecraft simultaneously, but each spacecraft collects, digitizes, and stores data independently of the rest of the constellation. Light which enters the telescope is coupled into a single mode fiber, which preserves the amplitude and phase information gathered from the optical field. This signal light, as well as light from the optical frequency comb are coupled into a photonic integrated circuit (PIC) where they can be mixed in a controlled fashion.

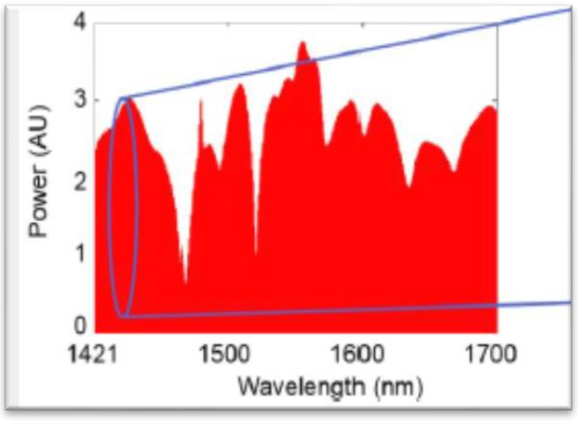

Figure 28: Plot of the measured spectrum for an optical frequency comb at Ball Aerospace. The individual lines can't be resolved at this scale, but spectral power is clearly visible over a wide range of wavelengths.

The PIC is used to break the field, now consisting of both light from the star and from the frequency comb (**Figure 28**), into frequency channels of $\Delta\nu = 1GHz$ bandwidth. Due to the repetitive nature of the frequency comb channel, this arrangement can be maintained continuously over two full octaves, spanning from 500nm to 2000nm in wavelength (A small portion of this spectrum is shown in **Figure 29**). Each channel can be custom designed, maximizing for throughput efficiency by optimizing each channel based on its center wavelength.

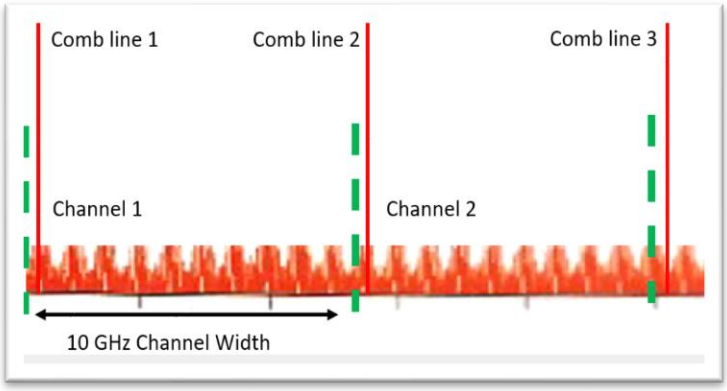

Figure 29: Illustration of a laser frequency comb, yielding phase coherence local oscillators at each of our (nominally) 10 GHz spectral channels.

The light in each channel is detected with a photon-counting detector which is sensitive to the output represented classically and semi-classically as:

$$\left|\vec{E}_{LO}+\vec{E}_{Sig}\right|^2=\left|\vec{E}_{LO}\right|^2+\left|\vec{E}_{Sig}\right|^2+2\left|\vec{E}_{LO}\vec{E}_{Sig}\right|^2=\dot{n}_{LO}T_0+\dot{n}_{Sig}T_0+2\sqrt{\dot{n}_{LO}\dot{n}_{Sig}}\cos\phi \quad (27)$$

Here $\vec{E}_{LO}$ represents the LO field, $\vec{E}_{Sig}$ represents the field collected from the astronomical target, $\dot{n}_{LO}$ represents the photon flux rate from the LO, and $\dot{n}_{Sig}$ is the photon flux rate from the astronomical target. The integration time, t_0, must be less than or equal to the optical coherence

time $t_c = 1/\Delta\nu$. Finally, the phase angle of the signal from the astronomical target relative to the LO generated by the frequency comb is represented by ϕ.

One possible method to get both amplitude and phase from the signal term is to perform in-phase and quadrature detection. This method requires the signal light be split into two streams before mixing. The first stream will be mixed directly with the LO, while the second stream will be mixed with a copy of the LO that has undergone a 90-degree phase delay. In principle, the phase shift can be applied to either the LO or signal streams, but because the LO stream's optical power can be controlled as a free parameter, manipulations will be made to the LO instead of the signal stream.

Measurement of the two detected signals allows construction of the signal phasor for each telescope:

$$z_k = A_k e^{i\phi_k} \tag{28}$$

Simultaneous measurement of the phasors z_1 and z_2 at two separate telescopes allows the optical field values to be averaged over a given t_0. Direct comparison of these averages between telescopes gives a measurement of the correlation of the phase of the optical field between the two points.

While the SRSAII system has many parallel channels at each telescope, the SNR of the signal is <<1 for any individual channel within a single t_c. Averaging phasor value longer than t_c results in degradation of the signal due to the coherence properties of light. This requires that the product $z_1 z_2^*$, which preserves the measured amplitude at each telescope and finds the relative phase difference, be calculated for each every t_c independently.[5] The phase differences between telescopes calculated for each t_c can then be averaged over long observation times, T_{obs}, resulting in:

$$\langle z_1 z_2^* \rangle = I_{12} e^{i\phi_{12}} = \gamma_{12} I_{LO} I_{Sig} e^{i\phi_{12}} \tag{29}$$

The signal intensity from the target and that from the LO are multiplied by the visibility function γ_{12}, which represents the degree of correlation of the signal light across the 1-2 baseline. The $\langle z_1 z_2^* \rangle$ allows direct measurement of γ_{12} which, as discussed in Section 4.5, is the primary measured quantity for an interferometer and allows construction of the image of the source through the relationships described in the Van Cittert-Zernike theorem.[36]

Because phasor measurements at each telescope are digitally stored independently of the other telescopes, post processing allows the $z_n z_m^*$ product to be made for every possible combination of telescopes within the constellation. Unlike direct detection interferometry, where the number of possible baselines is determined by the initial design of the optical beam combiner, a digitally correlating heterodyne system can add and remove telescopes throughout its mission. This allows a single system to respond to changes in observation targets or requirements and allows for capability upgrades during the course of a mission lifetime. The digital nature of the correlation used by SRSAII also allows spacecraft control errors and drifts to be compensated in post-processing using nanometer-class positional metrology, improving final SNR compared to a real-time system.

5.1. Metrology

Several classes of precision metrology are required for SRSAII to function. The below sections provide brief introduction to three most critical techniques.

5.1.1. Two Way Time and Frequency Transfer

The optical phase of all of the frequency comb LOs in the SRSAII constellation must be synchronized to a common reference. Techniques developed at NIST and in university laboratories have demonstrated phase synchronization of optical references via free-space propagation and coherent detection of optical frequency combs. Despite free-space paths of multiple kilometers, it has been shown that significant optical disturbances can be rejected, allowing LO synchronization with the accuracy and precision anticipated to be necessary for the SRSAII system.

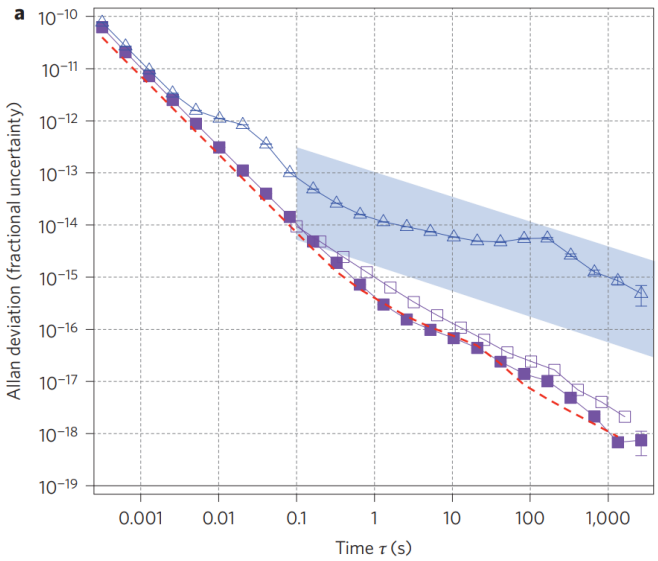

Figure 30: Allan Deviation of a frequency comb based optical two-way time and frequency transfer. This plot shows that two disparate optical oscillators can be stabilized to one another to better than one part in 10^{18}. This corresponds to phase stability on the order of milliradians.[37]

5.1.2. Spacecraft Control and Displacement Metrology

The SRSAII architecture greatly reduces the requirements that drive the traditional problem of controlling the distance between sub-aperture pairs to nanometer-class tolerances. Digital data collection and signal cross-correlation in post-processing allows correction of positional errors, which means that *knowledge* of the position of the spacecraft relative to the constellation is sufficient for operation.

Commonly achieved relative spacecraft positioning on the order of centimeters will be sufficient when paired with nanometer-class ranging measurements that leverage the phase stability of the on-board optical frequency combs. Such techniques have been demonstrated over free-space links, exhibiting nanometer precision with integration times on the order of 10s of milliseconds.[38]

5.1.3. Proof Mass Reference

Precision ranging is sufficient for relative spacecraft position within the constellation, however it is also necessary to measure rotations of the spacecraft constellation itself. As with the other orbital and mechanical displacements, errors in the rotation of the spacecraft constellation, which can lead to piston errors may be eliminated algorithmically in post-processing. To facilitate this, it may be necessary to implement three-axis accelerometers based on the Drag-Free and Attitude Control System (DFACS) designed for LISA. Future system level study will determine whether this is necessary on each spacecraft or only a single reference spacecraft. [39]

5.2. Constellation Configuration

In order to ensure continuous knowledge of the constellation, frequency comb-based nanometer ranging will be used for all measurements. In-plane measurements (**Figure 31**, green) will determine the x-y location of the imaging spacecraft, and out of plane measurement (Figure 31, red) will provide the z-direction measurements relative to the reference spacecraft. Placement of a proof-mass reference at the reference spacecraft should provide sufficient knowledge of the constellations rigid body motions in free space (i.e. those motions not accounted for by the inter-satellite ranging system).

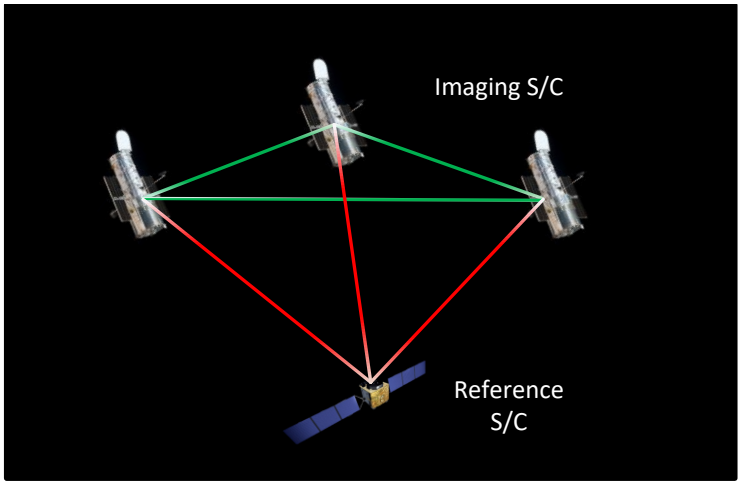

Figure 31: Laser metrology between imaging spacecraft, and with a reference spacecraft, will yield sufficient knowledge of constellation geometry for data correlation.

5.3. Detection Technologies

5.3.1. Collecting Optics

The SRSAII system is agnostic to the type of collection optics utilized. Traditional monolithic optics provide a low-risk approach and are sufficient for smaller collecting areas. To increase system sensitivity, however, it is possible to exploit recent developments in membrane optics technology. In the early 2010s, DARPA funded the MOIRE program to create imaging systems with lightweight membranes serving as primary optics (**Figure 32**). The program was successful in many ways, and Ball Aerospace has demonstrated image collection through a 1/8th section of a 5-meter membrane optic. Final designs scaled the optic to 20-meters, with an aperture fill-factor on the order of 50%.

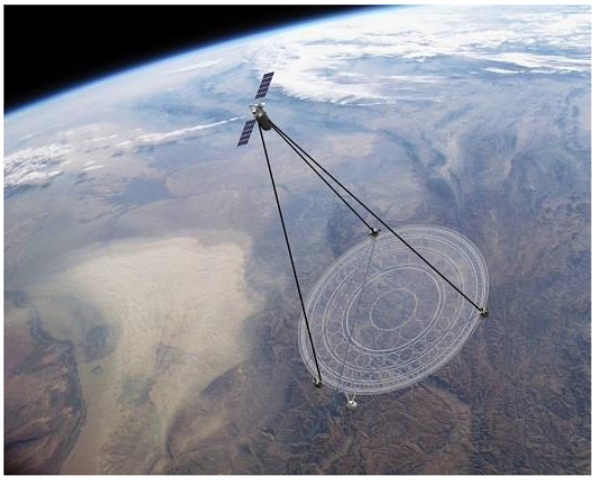

Figure 32: Artist's conception of a large space-based membrane telescope.[40]

As is typical with membrane optics, chromatic dispersion limited the bandwidth to a relatively narrow passband. For a SRSAII implementation, however, such chromatic dispersion can be designed to serve as the first stage of the necessary optical channelization, potentially increasing efficiency.

Implementation of the DARPA-funded membrane optic could serve to decrease SWAP by an order of magnitude when compared to traditional optics. Analyses in this report use 1.5m as the standard optical diameter, however designs for DARPA's applications scaled to 10m radius. Increasing from 1.5m to 10m improves sensitivity by 4 visual magnitudes, but likely begins to tax the other system trades. Further study on optical design and size is necessary.

5.4. Photonic Integrated Circuits

In the last several decades, Photonic Integrated Circuits (**Figure 33**) have emerged as a powerful and versatile tool for the miniaturization of optical capabilities, much like how ICs have revolutionized electronics. The capabilities of PICs span far and wide, ranging from light generation and detection, to routing, modulation, delay, filtering, and other aspects of signal processing. PICs have been shown to be a key technology enabler as signal routing and processing demands drive towards higher data rates, lower SWaP, and lower cost. Many of the processes needed for SRSAII, including signal channelizatifon, frequency comb generation, optical combining, and potentially even detection can take place on a PIC. [41,42]

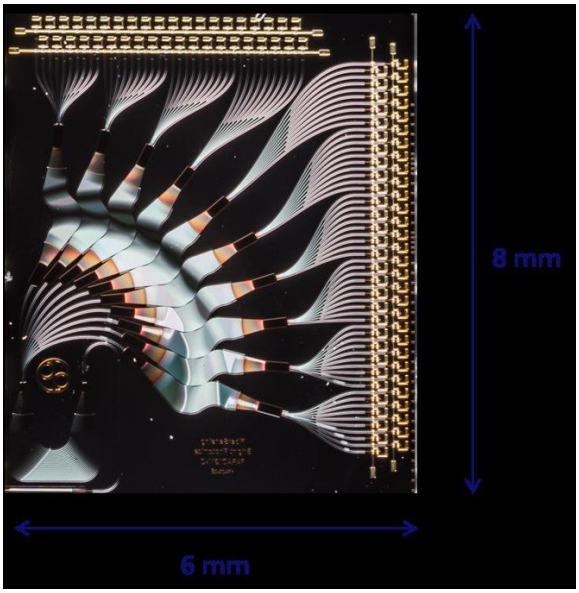

Figure 33: 6mm x 8mm PIC showing 100 optical channels which have been isolated and independently detected. The SRSAII system would require 100 PICs of similar nature and scale to the one shown here.[12]

5.4.1. Channelization

Thermal light collected by SRSAII must be broken into many frequency channels before coherent detection can be made. While the exact channel width is an open trade at the end of the Phase 1 efforts, it is expected that 1-10GHz will be ideal for this application. Current laboratory efforts for similar techniques have demonstrated 50GHz channel spacing as shown in **Figure 34**. Requirements and techniques will be determined for a future architecture study and narrowing the optical channels to the necessary widths is not expected to be of great technical difficulty.

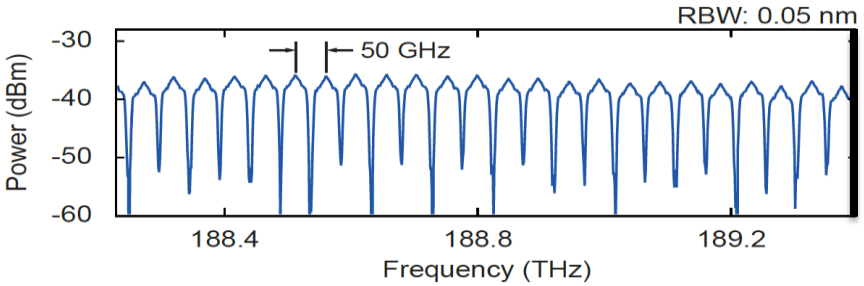

Figure 34: Many parallel optical channels created using PICs. This real-world implementation was created for laser communications, but could also be made to work for SRSAII.[43]

5.4.2. Frequency Comb LO

The subject of the 2005 Nobel Prize in Physics, optical frequency combs derive their name from the characteristic frequency spectrum which results from an ultrafast pulsed laser. This spectrum is the natural result of a mode-locked laser, and this frequency spectrum is directly related to the time-domain properties of the laser: The teeth are evenly spaced in frequency and their separation is driven by the repetition rate of the laser pulses. The number of teeth in the natural spectrum is driven by the duration of the pulse – the shorter the pulse, the greater the number of teeth. Spectral broadening is applied to the pulses and used to increase the spectral width from approximately 10nm to over 1µm, resulting in more than an octave of coverage.

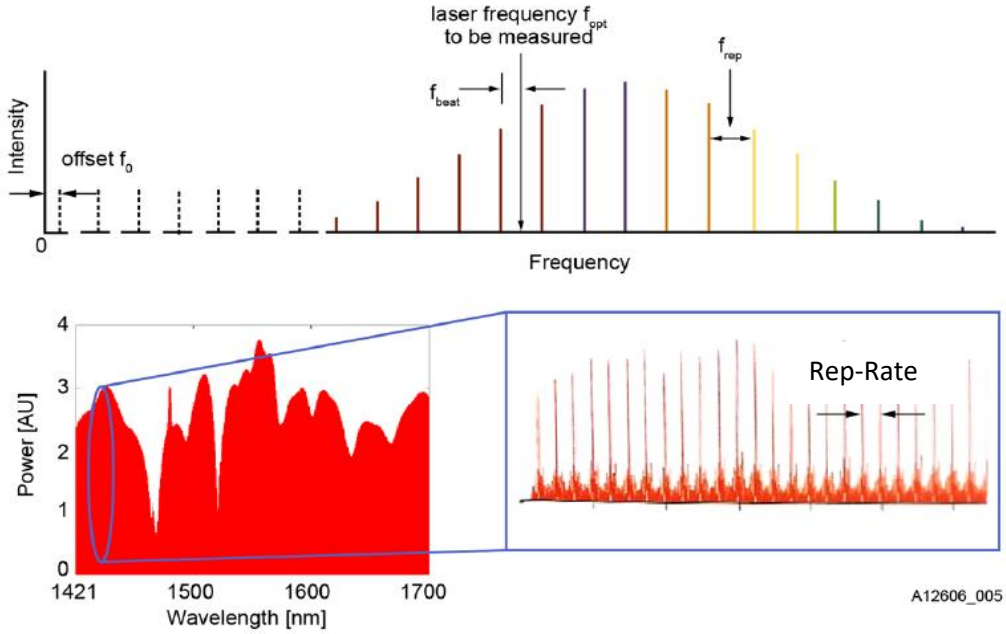

Figure 35: Optical frequency comb schematic showing the spectral width and repetitive spectrum critical to the comb's functionality.[44]

The spectrum of a frequency comb (**Figure 35**) can be stabilized such that all teeth are mutually phase-locked, giving an octave of equally spaced phase-coherent local oscillators. Multiplexing each comb-tooth with a single SRSAII channel, as shown in **Figure 36**, allows coherent detection of large, continuous portions of the optical spectrum.

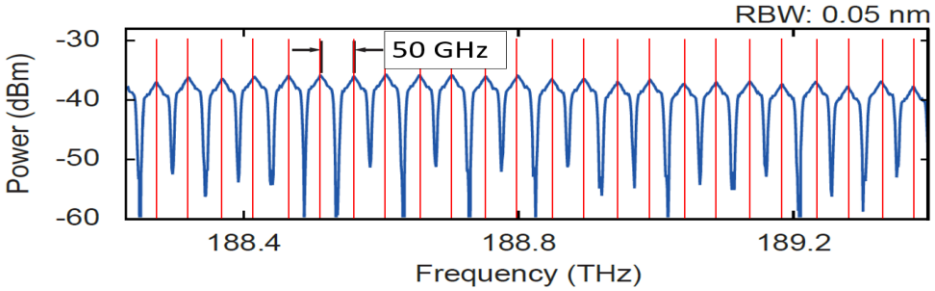

Figure 36: Optical frequency comb lines (red) spectrally aligned and mixed with optical channels (blue).[43,44]

5.5. Photon Counting and Data Rates

Critical to the detection scheme being proposed for SRSAII, the detectors must be able to time-tag single photons with temporal precision that corresponds to the inverse of the channel bandwidth. Sampling a heterodyne signal with $^{1}/_{20GHz} = 50\ picosecond$ time precision, for instance, effectively meets the Nyquist criterion for a signal of 10GHz. The benefit of sampling with a time precision of 50ps rather than at a rate of 20GHz becomes apparent when measuring a discontinuous signal.

For the photon starved regime in which SRSAII will operate, a total flux of 1000 photons per second results in 1000 samples per second, rather than 20e9 samples with a traditional detection scheme. When extrapolating this improvement from a single channel to the full NIAC system with ~10^4 channels results in an expected total sample rate on the order of 10^6 rather than 10^{15} samples as would be necessary with a traditional continuous detection scheme.

Conservatively bounding the system by assuming each optical sample is accompanied by less than 1000 bits, the resulting throughput is less than 1Gbit/sec. This data rate is manageable with current ethernet technology, and therefore will pose little challenge to future system implementation.

5.5.1. Photon Counting Detectors

Kovalyuk et al demonstrated a superconducting nanowire single photon detector (SNSPD) for coherent detection of very low signals.[45] SNSPDs provide high detection efficiency (>80% quantum efficiency) with low noise (<100 Hz) and high speed (order 10ns dead time, order 10 ps jitter). SNSPDs achieve high detection efficiency by exploiting geometry: by overlaying a nanowire on a waveguide in a dense pattern, one can increase the optical mode overlap with the nanowire. The timing accuracy (and thus detection bandwidth) is fundamentally limited by the photon counting jitter, corresponding to detection bandwidth of order 10 GHz.[46] Kovalyuk points out that the SNSPD demonstrates much lower noise and higher speed compared to other common single photon detectors (eg. Transition edge sensors or avalanche photodiodes). Kovalyuk demonstrated for their SNSPD detector design, heterodyne detection SNR was optimized for LO powers of ~10^4 photons, and that coincided with the smallest signal level detectable (order single photons)

6. Conclusion and Recommendations for Future Work

The SRSAII study investigated several interferometry techniques, each with its own unique benefits and drawbacks. At the close of the NIAC Phase I study, it is recommended that a follow-on study be performed through NIAC to investigate the systems trade space surrounding a multi-channel heterodyne interferometer intended to optically resolve diameter, aspect ratio, spectral content, and surface structure for astronomical targets as deep as 15th magnitude.

6.1. Multi-Channel Intensity Interferometry

This technique results in the lowest SNR for any of those studied. In addition, 2nd order intensity interferometry is insensitive to surface structures of its targets. An observatory intended to measure surface structure on astronomical targets must rely on 3rd order intensity correlations, which exhibit an SNR that is significantly poorer even than that of the 2nd order. In order to counteract low SNR values, it is necessary to implement large collecting optics which are likely to be cost prohibitive for implementation in space-based architectures.

Benefits of this technique include the ability to use optical telescopes that are significantly degraded from the diffraction limit. This allows for potentially cost-effective ground-based systems, or adaptation of an intensity interferometer to existing optical arrays not originally intended for interferometry, such as the Cherenkov Telescope Array.[47] Implementation of a SRSAII-derived multi-channel approach could further improve the SNR picture by as much as a factor of 100 for a fixed optical collection area. This results in the decrease of the required observation time to achieve a meaningful SNR by a factor of 10^4.

Further study of intensity interferometry is not recommended for funding under a SRSAII-related grant under NIAC, however collaboration with PIs of current intensity interferometry efforts may prove beneficial.

6.2. Quantum Assisted Interferometry

The first principles approach to the SNR derivation used in this study revealed an unanticipated path toward extremely high performance optical interferometry, and future implementation of techniques of this nature will likely prove significantly more capable than any other technique.

The nascent state of the technologies related to quantum computation and the complexities of quantum information theory will prove to be significant challenges when designing a system to implement this technique. At this point in time, meaningful experimental demonstration at the system level is unlikely to be feasible on the budget associated with a NIAC grant.

Despite its challenging nature, this technique promises to be extremely powerful and results in an SNR picture that rivals traditional beam-combination interferometry but also includes the added benefits of a digital system such as the ability to cross correlate measured signals in post-processing. As with all the techniques examined in the SRSAII phase I study, there is no need for real-time data correlation or extremely precise control of spacecraft constellations, which greatly decreases aerospace system complexity.

The significant departure of the truly quantum-mechanical operations in this technique from that of the primary architecture studied in the SRSAII Phase-I renders this technique primarily out of scope for this study. As such, it was not investigated in great enough detail to recommend for funding under a SRSAII-related phase II grant under NIAC. Due to the significant potential of this technique, however, it is strongly recommended for consideration by the NIAC program for phase 1 study.

6.3. Multi-Channel Heterodyne Interferometry

Space-Based multi-channel optical heterodyne interferometry as investigated by the SRSAII study is a promising technology which offers a viable path toward long baseline optical interferometry. While the SNR falls short of direct detection (homodyne) interferometry, critical advancements in optical physics and detector technology allow the SRSAII technique to bypass the most significant challenges of direct detection. Using this technique, an interferometer with nearly arbitrarily long baselines and sensitivity out to the 15th magnitude could be designed and flown in the next twenty years. Such unprecedented capability will allow the scientific community to directly resolve astronomical targets both spatially and spectrally, representing significant improvement over current optical domain techniques.

The primary benefits of this technique stem from the ability to correlate optical field measurements across long baselines without the need to control the spacecraft position to optical tolerances or combine multiple free-space beams onto a single detector. This greatly decreases system complexity and improves mission flexibility as spacecraft can be added, removed, or re-configured mid-mission without requiring changes to the optical system. Implementation of the SRSAII multi-channel optical heterodyne system improves the SNR when compared to a single channel heterodyne system by approximately the square root of the number of channels implemented. Leveraging Photonic Integrated Circuit (PIC) technology instead of an optical fiber architecture significantly decreases system scale, offering a form factor improvement similar to that seen in moving from discrete electrical components to integrated circuits. This critical advancement has the potential to enable hundreds of thousands of parallel channels in a small, manufacturable package, resulting in SNR improvements of a hundred fold or more when compared to current techniques.

Further study of this architecture is strongly recommended. The rapid pace of PIC and detector development should make a laboratory implementation of the SRSAII architecture viable within ten years, with a flight system following within 20-25 years. The scientific potential of a real-world SRSAII system capable of resolving 15th magnitude objects with multi-kilometer baselines is enormous.

7. References and Citations

[1] Newbury, N.R. (2011). Searching for applications with a fine-tooth comb. Nature Photonics, 5(4), 186-188. Doi:10.1038/nphoton.2011.38

[2] Malvimat, V., Wucknitz, O., & Saha, P. (2013). Intensity interferometry with more than two detectors? Monthly Notices of the Royal Astronomical Society, 437(1), 798-803. doi:10.1093/mnras/stt1934

[3] Wentz, T., & Saha, P. (2014). Feasibility of observing Hanbury Brown and Twiss phase. Monthly Notices of the Royal Astronomical Society,446(2), 2065-2072. doi:10.1093/mnras/stu2206

[4] Burke, B. F. (1969). Quantum Interference Paradox. *Nature,223*(5204), 389-390. doi:10.1038/223389a0

[5] J. B. Ashcom, "White Light Interferometry SNR", MIT Lincoln Laboratory Project Report LSP-132, 9 April 2015.

[6] Ball Aerospace & Technologies Corp. (2013, December 06). Ball Aerospace Demonstrates Ultra-Lightweight Telescope. Retrieved from http://www.coloradospacenews.com/ball-aerospace-demonstrates-ultra-lightweight-telescope/

[7] NASA Interim Report – The Large UV Optical Infrared Surveyor arXiv:1809.09668

[8] Barrett, H. H., & Myers, K. J. (2004). Foundations of image science. Hoboken, NJ: Wiley

[9] Rinehart, S. (2010). The Balloon Experimental Twin Telescope for Infrared Interferometry (BETTII). Optical and Infrared Interferometry II. doi:10.1117/12.855476

[10] NASA. (n.d.). Retrieved December 12, 2018, from https://www.nasa.gov/sites/default/files/m51.jpg

[11] Group, C. W. (2006, May 16). Retrieved December 12, 2018, from https://www.cfa.harvard.edu/sma/research/imageGallery/sciPages/m51/

[12] Community Access to the CHARA Interferometer on Mt. Wilson. (n.d.). Retrieved from https://www.noao.edu/gateway/chara/

[13] TP-6: InP-based Photonic Integrated Circuits (PICs) or Chips. (2018, January 29). Retrieved December 8, 2018, from http://www.actphast.eu/technology-platform/tp-6-inp-based-photonic-integrated-circuits-pics-or-chips

[14] Bouman, K. L., Johnson, M. D., Zoran, D., Fish, V. L., Doeleman, S. S., & Freeman, W. T. (2016). Computational Imaging for VLBI Image Reconstruction. 2016 IEEE Conference on Computer Vision and Pattern Recognition (CVPR). doi:10.1109/cvpr.2016.105

[15] Loudon, R. (1984). The Quantum Theory of Light. Oxford: Clarendon Pr.

[16] Tan, P. K., et al. (2014). Measuring Temporal Photon Bunching In Blackbody Radiation. The Astrophysical Journal,789(1). doi:10.1088/2041-8205/789/1/l10

[17] S.K. Saha, Aperture Synthesis, Astronomy and Astrophysics Library

[18] Born, M., Wolf, E., & Bhatia, A. B. (2016). Principles of optics electromagnetic theory of propagation, interference and diffraction of light. Cambridge: Cambridge Univ. Press.

[19] Haniff, C. (2007). An introduction to the theory of interferometry. New Astronomy Reviews,51(8-9), 565-575. doi:10.1016/j.newar.2007.06.002

[20] Goodman, J. W. (2005). Introduction to Fourier optics. Greenwood Village, CO: Roberts &.

[21] Perley, R. A., Chandler, C. J., Butler, B. J., & Wrobel, J. M. (2011). The Expanded Very Large Array: A New Telescope For New Science. The Astrophysical Journal,739(1). doi:10.1088/2041-8205/739/1/l1

[22] Finley, D. G. (1998). Very Long Baseline Array (VLBA). In AccessScience. McGraw-Hill Education. https://doi.org/10.1036/1097-8542.YB980660

[23] Shapiro, J.H. "The Quantum Theory of Optical Communications." Selected Topics in Quantum Electronics, IEEE Journal of 15.6 (2009): 1547-1569. © 2009 IEEE

[24] L. Liu, H. Zhang, J. Guo, S. Zhao, and T. Wang, "Photon time-interval statistics applied to the analysis of laser heterodyne signal with photon counter," Opt. Commun., vol. 285, pp. 3820–3826, 2012.

[25] P. J. Winzer and W. R. Leeb, "Coherent lidar at low signal powers: Basic considerations on optical heterodyning," J. Mod. Opt., vol. 45, no. 8, pp. 1549–1555, 1998.

[26] C. C. Davis, "Single-Photon Optical Heterodyning," IEEE J. Quantum Electron., vol. QE-15, no. 1, pp. 26–29, 1979.

[27] T. Mehringer, S. Mährlein, J. von Zanthier, and G. S. Agarwal, "Photon statistics as an interference phenomenon," Opt. Lett., vol. 43, no. 10, pp. 2304–2307, May 2018.

[28] Brown, R. H., & Twiss, R. Q. (1956). A Test of a New Type of Stellar Interferometer on Sirius. Nature,178(4541), 1046-1048. doi:10.1038/1781046a0

[29] Wentz, T., & Saha, P. (2014). Feasibility of observing Hanbury Brown and Twiss phase. Monthly Notices of the Royal Astronomical Society,446(2), 2065-2072. doi:10.1093/mnras/stu2206

[30] Dravins, D., Lagadec, T., & Nuñez, P. D. (2015). Long-baseline optical intensity interferometry. Astronomy & Astrophysics,580. doi:10.1051/0004-6361/201526334

[31] Frequency Bands & Performance. (n.d.). Retrieved from https://science.lbo.us/facilities/vlba/docs/manuals/oss/bands-perf

[32] Tsang, M. (2011). Quantum Nonlocality in Weak-Thermal-Light Interferometry. Physical Review Letters,107(27). doi:10.1103/physrevlett.107.270402

[33] Khabiboulline, E. T., Borregaard, J., De Greve, K., & Lukin, M. D. (n.d.). Nonlocal Optical Interferometry with Quantum Networks. Retrieved from https://arxiv.org/pdf/1809.01659

[34] Khabiboulline, E. T., Borregaard, J., & Lukin, M. D. (n.d.). Quantum-Assisted Telescope Arrays - arxiv.org. Retrieved from https://arxiv.org/pdf/1809.03396.pdf

[35] Gottesman, D., Jennewein, T., & Croke, S. (2012). Longer-Baseline Telescopes Using Quantum Repeaters. Physical Review Letters,109(7). doi:10.1103/physrevlett.109.070503

[36] Barrett, H. H., & Myers, K. J. (2004). Foundations of image science. Hoboken, NJ: Wiley

[37] Giorgetta, F. R., Swann, W. C., Sinclair, L. C., Baumann, E., Coddington, I., & Newbury, N. R. (2013). Optical two-way time and frequency transfer over free space. Nature Photonics, 7(6), 434-438. doi:10.1038/nphoton.2013.69

[38] Coddington, I., Swann, W. C., Nenadovic, L., & Newbury, N. R. (2009). Rapid and precise absolute distance measurements at long range. Nature Photonics,3(6), 351-356. doi:10.1038/nphoton.2009.94

[39] Armano, M., et al. (2018, December 13). LISA Pathfinder Platform Stability and Drag-free Performance. Retrieved from http://export.arxiv.org/abs/1812.05491

[40] Messier, D. (n.d.). Ball Aerospace Reaches Milestone on New Super Sized Telescope. Retrieved from http://www.parabolicarc.com/2013/12/13/ball-aerospace-telescope/

[41] J. Wang and Y. Long, "On-chip silicon photonic signaling and processing: a review," Sci. Bull., vol. 63, no. 19, pp. 1267–1310, 2018.

[42] F. Kish et al., "System-on-Chip Photonic Integrated Circuits," IEEE J. Sel. Top. Quantum Electron., vol. 24, no. 1, pp. 1–20, 2018.

[43] Marin-Palomo, P., Kemal, J. N., Karpov, M., Kordts, A., Pfeifle, J., Pfeiffer, M. H., . . . Koos, C. (2017). Microresonator-based solitons for massively parallel coherent optical communications. Nature,546(7657), 274-279. doi:10.1038/nature22387

[44] Wachs, J., Leitch, J., Knight, S., Pierce, R., & Adkins, M. (2016). Development and test of the Ball Aerospace optical frequency comb: A versatile measurement tool for aerospace applications. Advances in Optical and Mechanical Technologies for Telescopes and Instrumentation II. doi:10.1117/12.2230006

[45] Kovalyuk, V., Ferrari, S., Kahl, O., Semenov, A., Shcherbatenko, M., Lobanov, Y., . . . Gol'Tsman, G. (2017). On-chip coherent detection with quantum limited sensitivity. Scientific Reports,7(1). doi:10.1038/s41598-017-05142-1

[46] M. Shcherbatenko et al., "Potential of a superconducting photon counter for heterodyne detection at the telecommunication wavelength," Opt. Express, vol. 24, no. 26, pp. 30474–30484, Dec. 2016

[47] Dravins, D., & Lagadec, T. (2014). Stellar intensity interferometry over kilometer baselines: Laboratory simulation of observations with the Cherenkov Telescope Array. Optical and Infrared Interferometry IV. doi:10.1117/12.2055131